Precambrian Research 431 (2025) 107937

Contents lists available at ScienceDirect

Precambrian Research

journal homepage: www.elsevier.com/locate/precamres

Research Paper

Pre-Mesoproterozoic crustal framework and Mesoproterozoic evolution of the SW Angolan Shield: structural, geochemical, and isotopic insights from the Kunene Complex and surrounding basement

Enrique Merino-Martínez [a,*], Ezequiel Ferreira [a,c], Pablo Valverde-Vaquero [a], José Feliciano Rodrigues [b], Javier Escuder-Viruete [a], José Luis García-Lobón [a], Aratz Beranoaguirre [c,d], María del Carmen Feria [e], Carmen Rey-Moral [a], Paulo Bravo Silva [b], Pablo González-Cuadra [c], João Carlos Sousa [c], Julián Potti [c], Jaime Máximo [c], Miguel Gutiérrez-Medina [c], Juan Carlos Gumiel [a], Gustavo Galán [c], Tania Mochales [a], José Manuel [f], Domingos Cordeiro [f], Colombo Tassinari [g], Pilar Montero [h], Kei Sato [g], José Manuel Fuenlabrada [i], Carmen Galindo [i]

[a] Instituto Geológico y Minero de España (IGME), CSIC, c/ Ríos Rosas 23, 28003 Madrid, Spain
[b] Laboratório Nacional de Energia e Geologia (LNEG), Estr. da Portela 999, Amadora, Portugal
[c] UTE-PLANAGEO (IGME/LNEG/Impulso), Parque tecnológico de Asturias, parcela 13 A, 33428 Asturias, Spain
[d] Institut für Geowissenschaften, Goethe-Universität Frankfurt, Alternhöferallee 1, 60438 Frankfurt am Main, Germany
[e] Sistemas Avanzados de Tecnología, S.A (SATEC), Av. Europa, 34 A, 28023 Madrid, Spain
[f] Instituto Geologico de Angola (IGEO), Centralidade do Kilamba, Rua Nr, Luanda, Angola
[g] High Resolution Geochronological Laboratory, Geosciences Institute, University of São Paulo, Rua do Lago, 562, Cidade Universitária, CEP 05508-080 São Paulo, Spain
[h] SHRIMP Ion-Microprobe Laboratory - IBERSIMS. Centro de Instrumentación Científica. The University of Granada 18002 Granada, Spain
[i] Unidad de Geocronología, CAI de Ciencias de la Tierra y Arqueometría, Universidad Complutense de Madrid, c/ José Antonio Novais 2, 28040 Madrid, Spain

ARTICLE INFO

Keywords:
U-Pb geochronology
Kunene Complex
Mesoproterozoic magmatism
Kibaran belt
Archaean to Palaeoproterozoic crustal domains
Angolan Shield

ABSTRACT

The southwestern Angolan Shield hosts the Earth's largest Mesoproterozoic massif-type anorthosite complex (up to 53,500 km^2), the Kunene Complex (KC). This complex is the result of a long-lived (~200 Ma) episodic emplacement of coalescent magmatic pulses. The recent acquisition of multidisciplinary data during the PLANAGEO project has significantly enhanced our understanding of the Precambrian crustal framework from the southwestern Angolan Shield. Combined multi-isotope, structural and geophysical data reveals distinctive crustal zones in the southwestern Angolan Shield that clearly influenced KC's emplacement within a back-arc setting. The spatio-temporal arrangement of KC pulses suggests westwards magma migration within a complex contractional regime involving large strike-slip systems. A long-lasting and extensive accretionary orogen was responsible for the tectono-thermal activity recorded during most of the Mesoproterozoic. Crustal thinning and partial melting of isotopically heterogeneous lower-crustal sources through mantle upwelling promoted the episodic felsic magmatism contemporaneous with the KC. Crustal contamination processes are evident in gabbro-anorthosites, indicating mantle metasomatism and interaction with wall-rocks and granite melts during ascent, upwelled by lateral-driven forces. Deposition of extensive metasedimentary sequences (<1.26 Ga) covering the KC, along with 1.23–1.07 Ga sublithospheric and mantle-derived magmatism, indicate a shift from a compressional to an extensional regime during late-Mesoproterozoic times. Regional correlations with other Mesoproterozoic units in African and Brazilian counterparts suggest a shared geological evolution, despite potential differences in tectonic setting. These findings supports a refined geological model for the Mesoproterozoic evolution of the southwestern part of the Congo Craton.

* Corresponding author.
E-mail address: e.merino@igme.es (E. Merino-Martínez).

https://doi.org/10.1016/j.precamres.2025.107937
Received 23 February 2025; Received in revised form 29 September 2025; Accepted 30 September 2025
Available online 21 October 2025

1. Introduction

The petrogenesis and tectonic setting of Anorthosite-Mangerite-Charnockite-Granite (AMCG) complexes is still a matter of debate (e.g., Ashwal and Bybee, 2017; Sotiriou and Polat, 2023). The diverse petrographic, geochemical and structural relationships of these materials pose a significant challenge for explaining their provenance through conventional magmatic processes and achieving a unified genetic model (Ashwal, 1993). These igneous complexes have been ascribed to various geodynamic settings, including both extensional and compressional regimes. For example, Proterozoic anorthosites from the Dom Feliciano Belt of Brazil (Capivarita Anorthosite) are related to intracontinental extensional processes (Chemale et al., 2011), whereas anorthosites from Canada (Labrador Belt and Cross Lake-Pipestone Lake) and Central Australia (Musgrave orogen) are linked to a Proterozoic continental arc or back-arc settings (Smithies et al., 2011, Smits et al., 2014; Polat et al., 2022). The Rogaland Anorthosite Province of Norway has been related to both divergent and convergent scenarios (Duchesne et al., 1985; Slagstad et al., 2022).

In addition to the well-established association with mafic and ultramafic rocks, most anorthosite complexes are also associated with granitoid rocks (e.g., Elizondo-Pacheco et al., 2024). The high incompatible element contents and alkaline affinity of these rocks relate them to A-type granites, although S- and I-type granites are also commonly found (Milani et al., 2022). The coexistence of gabbro-anorthosite and granitoid rocks is an intriguing phenomenon that raises questions about whether they share common or separate origins. They could represent products of fractional crystallisation from the parental anorthositic magma; or they could derive from crustal melting under extensional conditions (Eby, 1992; Frost and Frost, 2011; Condie et al., 2023). However, isotopic and geochemical data often preclude a direct common origin for coeval anorthosites and A-type granites (e.g., Collins et al., 2019; Elizondo-Pacheco et al., 2024). This complexity underscores the need for integrative petrogenetic models that account for both mantle evolution and crustal processes across different tectonic regimes.

The Kunene Complex (KC), located in the SW Angolan Shield (Fig. 1), is the largest AMCG complex on Earth (42,500–53,500 km^2; e.g., Rey-Moral et al., 2022; Mochales et al., 2025), and is the result of protracted magmatism spanning at least 140 Ma (1500–1360 Ma; e.g., Mayer et al. 2004; Bybee et al., 2019; Milani et al., 2022). The exposed part of the KC (ca. 18,000 km^2; Figs. 1C, 2) forms an elongated, NNE-directed band that extends up to 350 km from the Namibian-Angolan border into Angola. Due to its petrological significance and economic potential, numerous studies have been conducted on the KC's main anorthositic, gabbroic and granitic lithotypes (e.g., Silva, 1990; Ashwal and Twist, 1994; Drüppel et al., 2000, 2007; Maier et al., 2013; Milani et al., 2022), although primarily limited to the exposed western portion of the Angolan KC and northwestern Namibia (Zebra Mountains).

The Archaean to Palaeoproterozoic basement that borders the Angolan KC remains largely unknown, particularly along the eastern

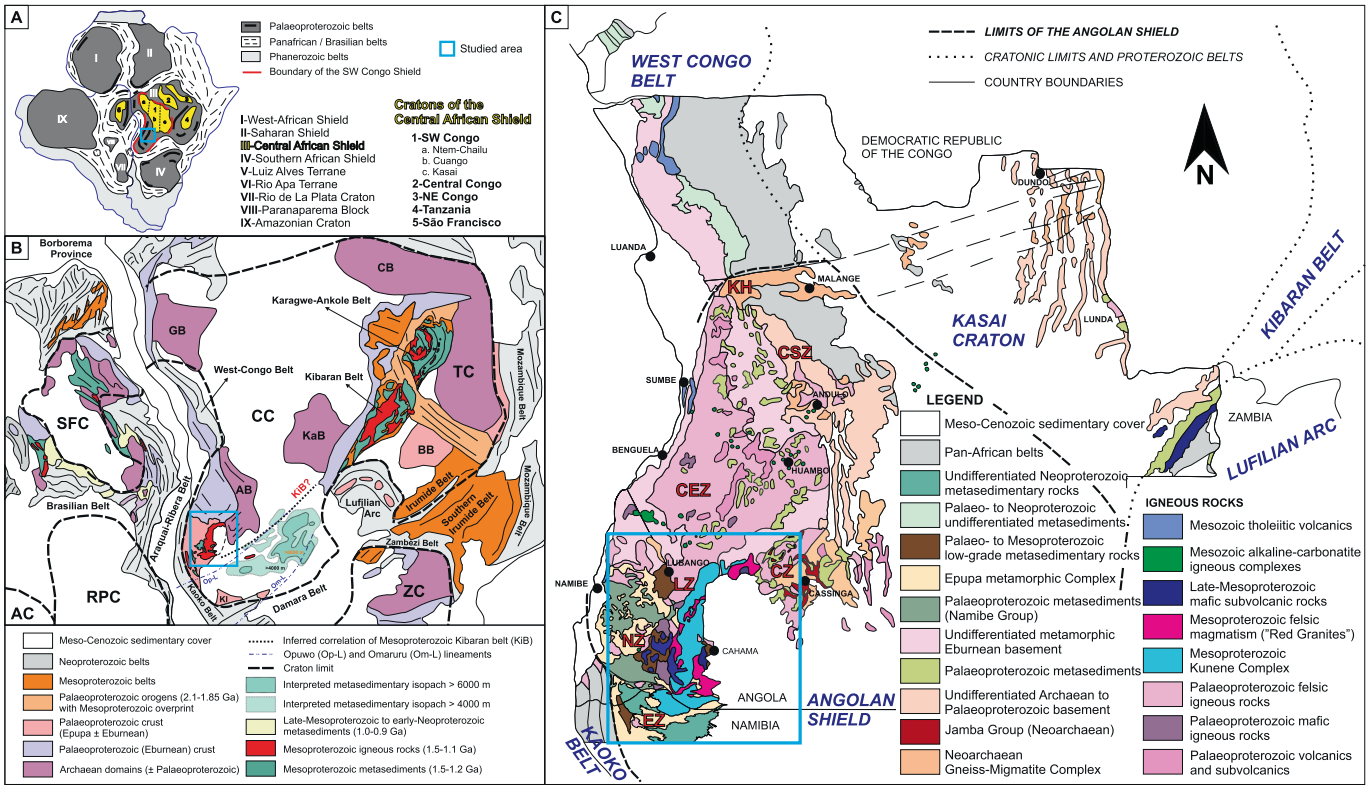

Fig. 1. A) Main Archaean cratons and terrains (grey) and Proterozoic orogenic belts of Africa and South America (modified from Siga Jr et al., 2011). Cratons forming the Central African Shield are highlighted in yellow (modified from De Wit and Linol, 2015). B) Reconstruction of southern Gondwana, highlighting the Mesoproterozoic rift-related sequences and Mesoproterozoic igneous rocks described in the Congo and São Francisco Cratons (modified from Marimon et al., 2020). It is also illustrated the interpreted extension of Meso- to Neoproterozoic deep sedimentary basins of Namibia and Angola, constrained between the magnetic Opuwo (Op-L) and Omaruru (Om-L) lineaments, overlaid by other possible younger sequences and the Kalahari cover (Corner and Durrheim, 2018). The yellow square frames the studied area of the present work. Abbreviations are as follow: AB, Angola Block, AC, Amazon Craton; BB, Bangweulu Block; CB, Congo Block; CC, Congo Craton; GB, Gabon Block; KaB, Kasai Block; KiB, possible extension of the Kibaran Belt under the Kalahari basin; SFC, São Francisco Craton; RPC, Rio da Plata Craton; TC, Tanzania Craton; ZC, Zambia Craton. C) Distribution of Archaean to Palaeoproterozoic domains and Proterozoic orogenic belts within the Congo Craton, showing the proposed crustal zones and/or geotectonic domains within the Angolan Shield (modified from Jelsma et al., 2018): KH, Kwanza Horst; CSZ, Central Shield Zone, CEZ, Central Eburnean Zone; CZ, Cassinga Zone; LZ, Lubango Zone; NZ, Namibe Zone; EZ, Epupa Zone). The blue squares indicate the location of the studied area, shown in Fig. 2.

boundary of the complex, despite the recent advances in the last decade (e.g., Pereira et al., 2011, 2013; McCourt et al., 2013; Bybee et al., 2019). Since 2015, the Angolan government has implemented an ambitious geological mapping project (National Geology Plan of Angola, PLANAGEO) to foster the countrýs geological infrastructure. As part of the PLANAGEO project, we conducted surveys covering the vast and remote regions of southwestern Angola, including the unexplored eastern areas of the KC in Angola and its host basement.

Distinct crustal tectonic domains have been proposed within the Angolan Shield (Carvalho et al., 2000; Jelsma et al., 2018), which have been recently updated through PLANAGEO's geological mapping (Fig. 1C; Rodrigues et al., 2021; Merino-Martínez et al., 2022). Rey-Moral et al. (2022) and Mochales et al. (2025) highlighted the distinct geophysical response of the basement surrounding the KC, suggesting that pre-Mesoproterozoic structures influenced the emplacement of the complex, as also described for other anorthositic provinces (e.g., Emslie et al., 1994). However, the geological evolution of the Angolan Shield during the Mesoproterozoic remains debated. While Mesoproterozoic magmatism in SW Angola and northwest Namibia has been traditionally interpreted as anorogenic (LIPs systems; e.g., Ernst et al., 2013, 2014), recent research suggesting a collisional setting for the Kunene Complex (e.g., Ashwal and Bybee, 2017; Bybee et al., 2019; Lehmann et al., 2020; Milani et al., 2022) opens new debate on the assembly and break-up of the Columbia supercontinent and the formation of Rodinia during the so-called "boring billion" (Roberts, 2013; Meert and Santosh, 2017). Similarly, the time-equivalent bimodal magmatism of the Kibaran Belt (Fig. 1B) has been attributed to both intracontinental extensional and convergent scenarios (e.g., Hanson, 2003; Kokonyangi et al., 2007; Tack et al., 2010). Nevertheless, a comparable and prolonged Mesoproterozoic geodynamic evolution has also been proposed for the African (Kibaran, Karagwe-Ankole and Northern Irumide Belts; Fig. 1B) and Brazilian counterparts (e.g., Fernandez-Alonso et al., 2012; Faleiros et al., 2024).

This study presents new multi-isotope and structural data for the KC and its surrounding basement, based on extensive geological investigations conducted in the PLANAGEO project. Twelve U-Pb zircon ages from the Archaean (2.67–2.57 Ga) to Palaeoproterozoic (1.99–1.97 and 1.80–1.77 Ga) basement, and ten age determinations from KC samples (1.45–1.34 Ga), complement the limited isotopic information for these underexplored regions. The petrogenetic discussion is enriched by comprehensive whole-rock geochemical and Sr-Nd isotope data from representative KC rocks. The additional U-Pb detrital zircon dating of the sedimentary cover sequence of the Kunene Complex (<1.26 Ga) provides valuable supplementary information that enhances the precision of the age data for other metasedimentary sequences from SW Angola (Ferreira et al., 2024). This integrated approach improves our geological understanding of the southwestern Angolan Shield, providing new insights into the emplacement of the Kunene Complex and the Mesoproterozoic evolution of the southern margin of the Congo Craton.

2. Geological setting

The studied area is located in southwest Angola and northwest Namibia, forming part of the Angolan Shield, at the southwestern

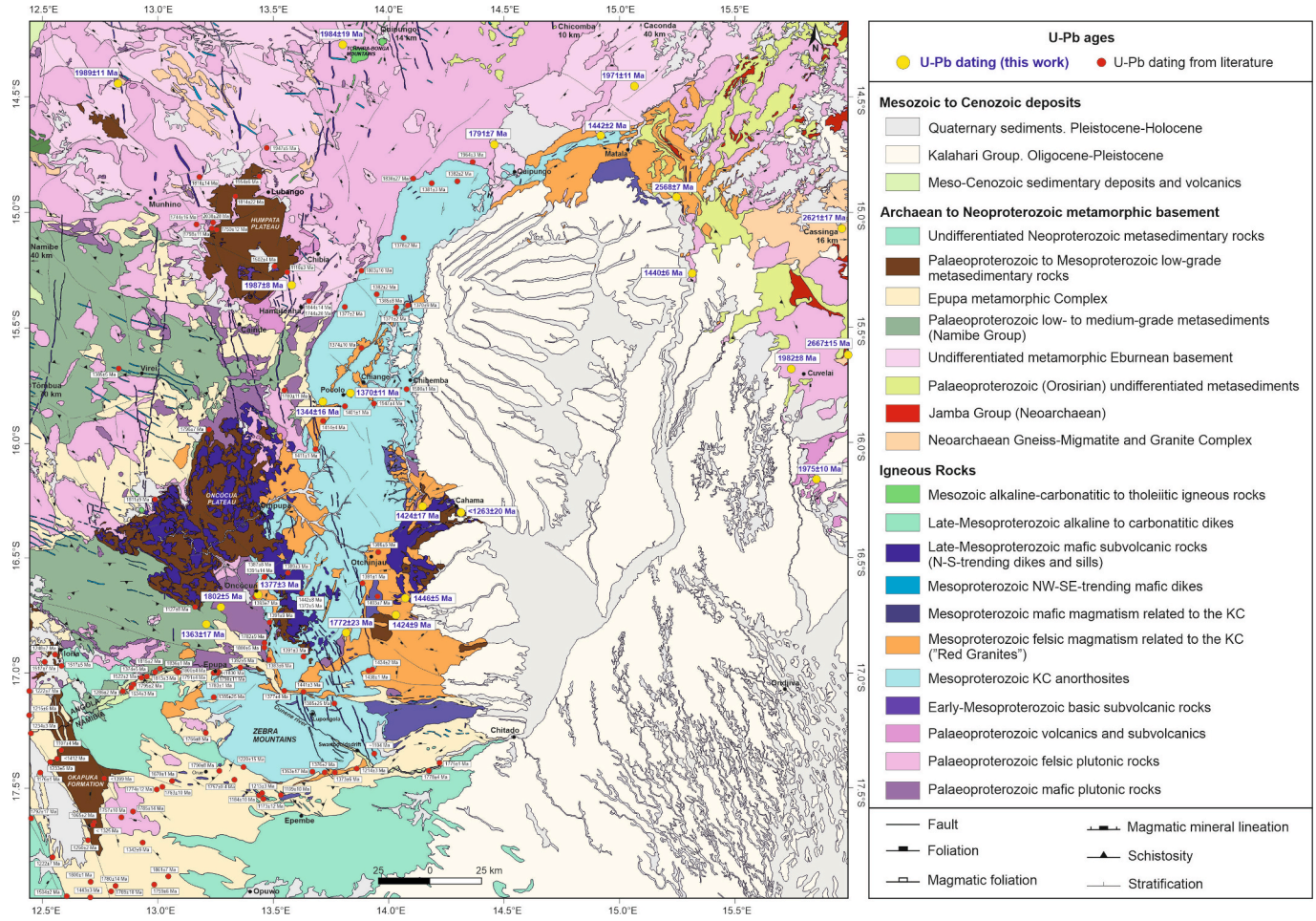

Fig. 2. Simplified geological map of the studied area, showing the main lithodemic units from SW Angola and NW Namibia and the distinct magmatic units found in the Kunene Complex. The location and U-Pb age values reported in the literature are shown in red circles, whereas the new U-Pb ages from this study are shown in yellow circles. The location of the analysed samples for whole-rock geochemistry is shown in green points (see Fig. S1 and Table S1 for sample details).

margin of the Congo Craton (Fig. 1). The Congo Craton is made up of distinct blocks or cratonic units, remnants of an Archaean crust, that were amalgamated throughout the Eburnean (ca. 2.1–1.8 Ga), Kibarian (ca. 1.5–1.0 Ga), Pan-African (ca. 0.8–0.5 Ga) orogenies (De Wit and Linol, 2015). The effects of these accretionary events are expressed as extensive deformation belts and peripheral suture zones, partially overlapped or disrupted, forming the Mesoproterozoic Karagwe-Ankole, Kibaran, and Irumide belts and the Neoproterozoic Western Congo, Mozambique, and Damara-Kaoko belts and the Lufilian Arc (e.g., De Waele et al., 2008; Tack et al., 2010; Fernandez-Alonso et al., 2012; Goscombe et al., 2017; Marimon et al., 2020; Fig. 1B).

The Angolan Shield is mainly composed of a metaigneous and metasedimentary Archaean to Palaeoproterozoic crust (Fig. 1C; Jelsma et al., 2018), partially intruded by Mesoproterozoic igneous rocks. Subsequent transpressive processes between the Congo and Rio de la Plata Cratons were responsible for the development of the Neoproterozoic (Pan-African) Kaoko Belt, which was later fragmented during the Mesozoic opening of the Atlantic Ocean (Fig. 1; e.g., De Waele et al., 2008; Evans and Mitchell, 2011; Meert, 2012; Goscombe et al., 2017). The geology of the studied area is summarised as follows (Fig. 2):

2.1. Archaean crust

The Archaean crust is represented by the Jamba Group and the Gneiss-Migmatite and Granite Complex (Carvalho 1982; Carvalho et al., 2000). The Jamba Group is composed of highly deformed low- to medium-grade metavolcanic and metasiliciclastic sequences interlayered with banded-iron formations (BIFs), structured as NNW-SSE to NNE-SSW oriented mega-syncline and anticline folds (Korpershoek, 1970, 1984; Pascal, 1980; Bassot et al., 1981; Sousa et al., 2021; Buzzi and Gutiérrez-Medina, 2022). The occurrence of the Jamba Group is limited to the east of the Kunene Complex, in the Cassinga Zone (Fig. 2; Carvalho and Alves, 1993; Jelsma et al., 2018). The Gneiss-Migmatite and Granite Complex is mainly composed of weakly foliated peraluminous to slightly metaluminous metagranites, locally migmatised, and rare metagabbros (Delhal et al., 1969, 1976; Carvalho, 1984). While covering wide areas in the Cassinga zone, the Archaean crust in the Central Eburnean Zone is essentially restricted to small remnants of ortho- and paragneisses within a dominant metaigneous Palaeoproterozoic crust (Fig. 2; Carvalho, 1982; Merino-Martínez et al., 2022).

2.2. Palaeoproterozoic crust

Palaeoproterozoic materials are major components of the Cassinga Zone and the Central Eburnean Zone (Fig. 1; e.g., Carvalho and Alves, 1993; Jelsma et al., 2018; Merino-Martínez et al., 2022). Metaluminous to slightly peraluminous granitoid rocks (traditionally regarded as the Eburnean Regional Granite; Pascal, 1980; Carvalho, 1982) are common constituents of this basement, together with rare gabbroic to dioritic bodies, intermediate to felsic (sub)volcanics and siliciclastic metasediments (Fig. 2; Carvalho and Alves, 1993; Silva and Caessa, 2021; Gutiérrez-Medina, 2022; Merino-Martínez and Goicoechea, 2022). The magmatic rocks display U-Pb zircon crystallisation ages ranging from 2.04 to 1.74 Ga (Pereira et al., 2011, 2013; McCourt et al., 2013; Jelsma et al., 2011, 2018; Langa, 2019; Milani et al., 2022; Campeny et al., 2023). These rocks show fragile-ductile and ductile deformation features, reaching up to medium- to high-grade metamorphic conditions (localised migmatisation), defining limited mobile belts (Torquato et al., 1979; Silva and Simões, 1980).

To the west and south of the Kunene Complex, the Palaeoproterozoic basement is dominated by the low- to medium-grade meta-volcanosedimentary sequence of the Namibe Group (previously known as the Schist-Quartzite-Amphibolite Complex; Carvalho and Alves, 1993; Silva, 2005; Escuder-Viruete et al., 2021; Silva et al., 2021), and medium to high-grade metamorphic materials of the Epupa Metamorphic Complex (EMC; Fig. 1; Miller, 2008). In NW Namibia, the EMC shows U-Pb protolith ages from 1.86 to 1.76 Ga, with ductile deformation and migmatisation coeval with the latest magmatic pulses (Kröner et al., 2010, 2015). This basement is partially covered by subhorizontal low-grade meta-volcanosedimentary sequences (Fig. 2), known as the Chela Group in the Humpata Plateau (1.80–1.75 Ga; Carvalho et al., 2000; Pereira et al., 2011, 2013; McCourt et al., 2013) and as the Ompupa and Iona Groups and Cahama and Okapuka Formations to the south of the Oncócua Plateau (1.32–1.18 Ga; Kröner and Rojas-Agramonte, 2017; Ferreira et al., 2024).

2.3. Mesoproterozoic crust

Distinct Mesoproterozoic igneous assemblages are found in the SW Angolan Shield, ranging in age from 1.53 to 1.07 Ga (e.g., Seth et al., 2005; Luft et al., 2011; Ernst et al., 2013, 2014; Maier et al., 2013; Kröner et al., 2015; Kröner and Rojas-Agramonte, 2017; Salminen et al., 2018; Ferreira et al., 2024). However, the most significant Mesoproterozoic magmatism is related to the intrusion of the Kunene Complex, mainly emplaced between 1.50 and 1.36 Ga (e.g., Mayer et al., 2004; Seth et al., 2005; Baxe, 2007; Drüppel et al., 2007; McCourt et al., 2013; Bybee et al., 2019; Lehmann et al., 2020; Milani et al., 2022).

The exposed part of the KC forms an elongated, NNE-directed band extending up to 350 km from the Namibian-Angolan border into Angola (ca. 18,000 km^2; Fig. 2). Anorthosites and gabbros, such as leucotroctolites and leuconorites, are the main lithotypes of the gabbro-anorthosite complex (e.g., Ashwal and Twist, 1994). Most KC anorthosites are unaltered and preserve primary magmatic textures (Slejko et al., 2002), although metasomatised textures and solid-state metamorphic structures are also profuse along the complex (referred as black and white anorthosites, respectively; Morais et al., 1998; Drüppel et al., 2007). Contemporaneous felsic magmas (commonly known as Red Granites) are found at the outer margins of the KC and in relatively narrow structurally controlled corridors within the complex (Fig. 2). These felsic lithologies include a variety of granite facies, including alkali-feldspar granites, quartz-monzonites, and quartz-syenites, as well as volcanic and subvolcanic materials, such as mangerites, rhyodacites, rhyolites, quartz-latites, quartz-trachytes and porphyritic microgranites, particularly in the Matala and Cahama regions (Torquato and Salgueiro, 1977; Carvalho and Alves, 1990, 1993; Escuder-Viruete and Gumiel, 2021; Galán, 2021; Potti, 2021). Distinct ductile deformational structures are described both in the anorthosites and granitoid members of the KC (Bybee et al., 2019; Lehmann et al., 2020, 2023; Milani et al., 2022).

Following the KC emplacement, magmatism resumed between 1.28 and 1.07 Ga, marking the end of Mesoproterozoic magmatism in the region. The resulting igneous rocks are essentially undeformed and consist of alkali-feldspar granites, alkaline-carbonatitic and tholeiitic rocks found in both SW Angola and NW Namibia (Fig. 2; e.g., Silva et al., 1973; Carvalho, 1984; Carvalho et al., 2000; Ernst et al., 2013; Kröner and Rojas-Agramonte, 2017; Salminen et al., 2018; Tshiningayamwe et al., 2022a; Ferreira et al., 2024).

3. Analytical methods

The studied samples were collected between 2016 and 2019 as part of PLANAGEO. A detailed description of the analytical methods can be found in the Supplementary Material. Whole-rock geochemical analyses of Mesoproterozoic samples were conducted in the facilities of ALS Chemex South Africa (Pty) Ltd., in Johannesburg (n = 26). Mesoproterozoic samples selected for geochronological purposes were also subjected to whole-rock geochemical (n = 5) and Sr-Nd isotope (n = 6) analyses, performed at the Bureau Veritas Commodities Canada Ltd (AcmeLabs; Vancouver, Canada), and in the Geochronology Unit of the Complutense University of Madrid (Spain), respectively. U-Pb dating was carried out by ID-TIMS at IGME-CSIC laboratories in Spain (n = 8)

with a Triton TIMS mass spectrometer and a ^{205}Pb-^{233}U-^{235}U spike, and by SHRIMP-IIe instruments at the High-Resolution Geochronological Laboratory of the University of São Paulo, Brazil (n = 6), and the IBERSIMS laboratory of the University of Granada, Spain (n = 9). Age plots and corresponding age calculations were performed using the Microsoft Excel add-in Isoplot® (Ludwig, 2012). All calculated age uncertainties are reported in the text, figures and tables at the 2σ level. Density plotter (Vermeesch, 2012) was used for the analysis of the U-Pb age distribution of detrital zircon. The full lithogeochemical and U–Pb analytical data are included in Tables S1 and S2. The location and the main mesoscopic features of the samples examined in this work are shown in Fig. 4 and Fig. S1.

4. Whole-rock geochemical features of KC materials

Representative gabbro-anorthosite units (n = 12) and felsic materials (n = 16) were sampled from the exposed western and the underexplored eastern segments of the KC (Fig. S1). Gabbro-anorthosite samples mostly consist of anorthosites and leucotroctolites, whereas the analysed felsic materials related to the KC are represented by both plutonic and volcanic facies, including distinct red granites, a syenite, a pegmatite, and diverse granite porphyries, microgranites and rhyodacites (Table S1).

Anorthosite rocks from both the eastern and western segments of the KC show low SiO_2 (45.5–55.7 wt%), Na_2O (0.9–4.8 wt%), and K_2O (0.1–1.7 wt%) contents; moderate CaO (3.3–12.95 wt%), high Al_2O_3 (7.7–28.7 wt%), and variable MgO (0.01–0.28 wt%), TiO_2 (0.1–1.5 wt %) and Fe_2O_{3t} (0.9–16.5 wt%) concentrations (Fig. S2). The studied samples are geochemically classified from the gabbro to monzodiorite compositional fields, varying from minor tholeiitic suites to dominant calc-alkaline series (Fig. 3A, B). These samples mostly show a metaluminous and magnesian affinity, although some weakly peraluminous and ferriferous terms are also found (Fig. 3C, D). The primitive mantle (PM)-normalised distributions exhibit a relatively flat multielement pattern, with an enrichment in LILE and a variable distribution of HFS elements (Fig. 3E). With the exception of an altered anorthosite, that clearly shows Rb enrichment due to metasomatic processes, they commonly show positive anomalies of Ba, Pb, Sr, Nd, and Eu, and negative of Rb, Nb, P, and Zr. The chondrite normalised REE diagram also shows a flat spectrum, with a slight enrichment in LREE contents and an almost flat to slightly depleted HREE patterns (Fig. 3G). A large positive Eu anomaly characterizes most gabbro-anorthosite samples, although a slightly negative to positive Eu-anomalies are found in some units from the western segment of the KC. The geochemical patterns are similar to those reported in other gabbroic and anorthosite materials from the exposed western and south-eastern segments of the KC (Figs. S2, S3; Baxe, 2007; Brower, 2017).

The studied felsic KC materials cover a wide compositional range of SiO_2 (54.9–83.5 wt%), Na_2O (0.8–7.3 wt%), K_2O (0.6–6.7 wt%); CaO (0.1–10.4 wt%), Al_2O_3 (9.8–22.7 wt%), MgO (0.04–5.80 wt%), TiO_2 (0.02–1.01 wt%), Fe_2O_{3t} (0.9–12.1 wt%) and P_2O_5 (0.01–0.23 wt%), commonly showing progressive depletion in Al_2O_3, Na_2O, CaO, TiO_2, MgO, Fe_2O_{3t} with silica increasing (Table S1). The distribution of Al_2O_3, K_2O, Na_2O, Sr and Ba in the felsic samples is characterised by a concave-down trend, showing a positive correlation with SiO_2 from ca. 53 to 68 wt%, and decreasing towards the most acidic terms (up to 83.5 wt% SiO_2; Fig. S2). Some granitoids and volcanic equivalents plot from the monzonite to syenite alkaline field; however, the majority of the samples have a subalkaline affinity, being classified from the diorite to granite geochemical fields (Fig. 3A). These subalkaline samples display both tholeiitic and calc-alkaline evolutionary trends (Fig. 3B). The KC felsic samples mostly exhibit a ferriferous character, evolving from metaluminous to peraluminous affinities with maficity decreasing (Fig. 3C-D).

The Sr/Y and $(La/Yb)_N$ ratios of the felsic KC materials mostly range from 0.05 to 41.09 and from 0.74 to 40.76 respectively (Fig. S4). The KC felsic materials display highly enriched LILE and LREE contents and the PM-normalised patterns are mostly defined by positive anomalies of Th, Pb and Zr and by marked negative anomalies of Ba, Nb, Sr, P, and Ti (Fig. 3F). Moderately steep REE chondrite-normalised patterns with marked negative Eu anomalies and flat HREE trends mostly characterise these materials (Fig. 3H). Despite the slightly distinct trends and anomalies from certain felsic samples (i.e., a granite and a granite pegmatite displaying lower LILE and LREE, and higher HFS and HREE, alike to that previously attributed to the M-type tetrad effect resulting from fluid-melt interaction; Milani et al., 2022), the overall patterns are analogous to those previously reported in other granitoids and KC-related felsic materials (Baxe, 2007; Kröner et al. 2015; Kröner and Rojas-Agramonte 2017; Milani et al. 2022).

5. Isotopic results

Samples selected for U-Pb geochronology include representative materials from the plutono-metamorphic basement surrounding the Kunene Complex, a basaltic dike intrusive into this basement, anorthosite rocks and distinct plutonic and volcanic felsic materials related to the KC, and a sedimentary rock overlaying the KC (Fig. S1). Cathodoluminescence (CL) images of representative zircon grains from samples dated by U–Pb SHRIMP and analytical spot locations are shown in Fig. S5. Two anorthosites samples and four felsic rocks from the Kunene Complex were selected for whole-rock Rb-Sr and Sm-Nd isotope analyses. In this section, we provide a brief outline of the lithological and structural characteristics, along with a summary of the U-Pb and Sr-Nd results obtained for the studied samples (Tables 1 and 2).

5.1. Archaean and Palaeoproterozoic basement of the Kunene Complex

5.1.1. Archaean materials from the Cassinga Zone

Dated samples representative of the Archaean plutono-metamorphic basement of the Cassinga area correspond to: a foliated porphyritic biotite granite (UTJPD33P044I) found alongside Mesoproterozoic red granites in the banks of the Cunene river; a biotite granite-gneiss (360/197/JFM) located ca. 18 km WNW of Cassinga; a porphyritic biotite granite-gneiss with large K-feldspar phenocrysts (UTMGD33X018I), collected approximately 20 km ENE of Cuvelai (Fig. 4). These granitoids exhibit variable mineral orientation and deformation, ranging from foliated to gneissic textures (Fig. S1). The foliation is marked by the alignment of biotite and the plastic elongation of feldspars and quartz. The distribution of the gneissic facies is highly heterogeneous, suggesting their association with regional shear bands. The measured orientations display irregular patterns, varying from NE-SW to NNW-SSE directions. The U-Pb data obtained for these samples reveal crystallisation ages of 2667 ± 15 Ma for sample UTMGD33X018I (MSWD = 0.35, upper intercept age; Fig. 5A), 2621 ± 17 Ma for sample 360/197/JFM (MSWD = 0.71, upper intercept age; Fig. 5B), and 2567.8 ± 6.8 Ma for sample UTJPD33P044I (MSWD = 1.4, concordia age; Fig. 5C).

5.1.2. Palaeoproterozoic Eburnean basement

Samples from the Palaeoproterozoic Eburnean-aged basement surrounding the Kunene Complex mainly consist of variably deformed porphyritic to equigranular granite facies (Fig. S1), frequently showing magma mingling textures. The deformational features found in these rocks are heterogeneous, both in intensity and in spatial distribution. Isotropic to weakly foliated facies often gradually transition to intensely deformed zones, showing gneissic layering to schlieric textures, occasionally evidencing partial melting conditions.

The basement to the northwest of the KC is represented by the following samples: a NW-SE to NNW-SSE trending biotite-rich schlieric granite (UTEMD33N159I) and a foliated porphyritic granite (UTMGD33M135I) located ca. 80 to 90 km to NNE and NW of Lubango, respectively; and a NNW-SSE trending biotitic granite-gneiss (356/62/PB), located a few kms southeast of the Humpata Plateau (Fig. 4; Fig. S1). U-Pb data for these samples indicate crystallisation ages of 1984 ± 19 Ma (MSWD = 0.22; upper intercept age), 1989 ± 11 Ma,

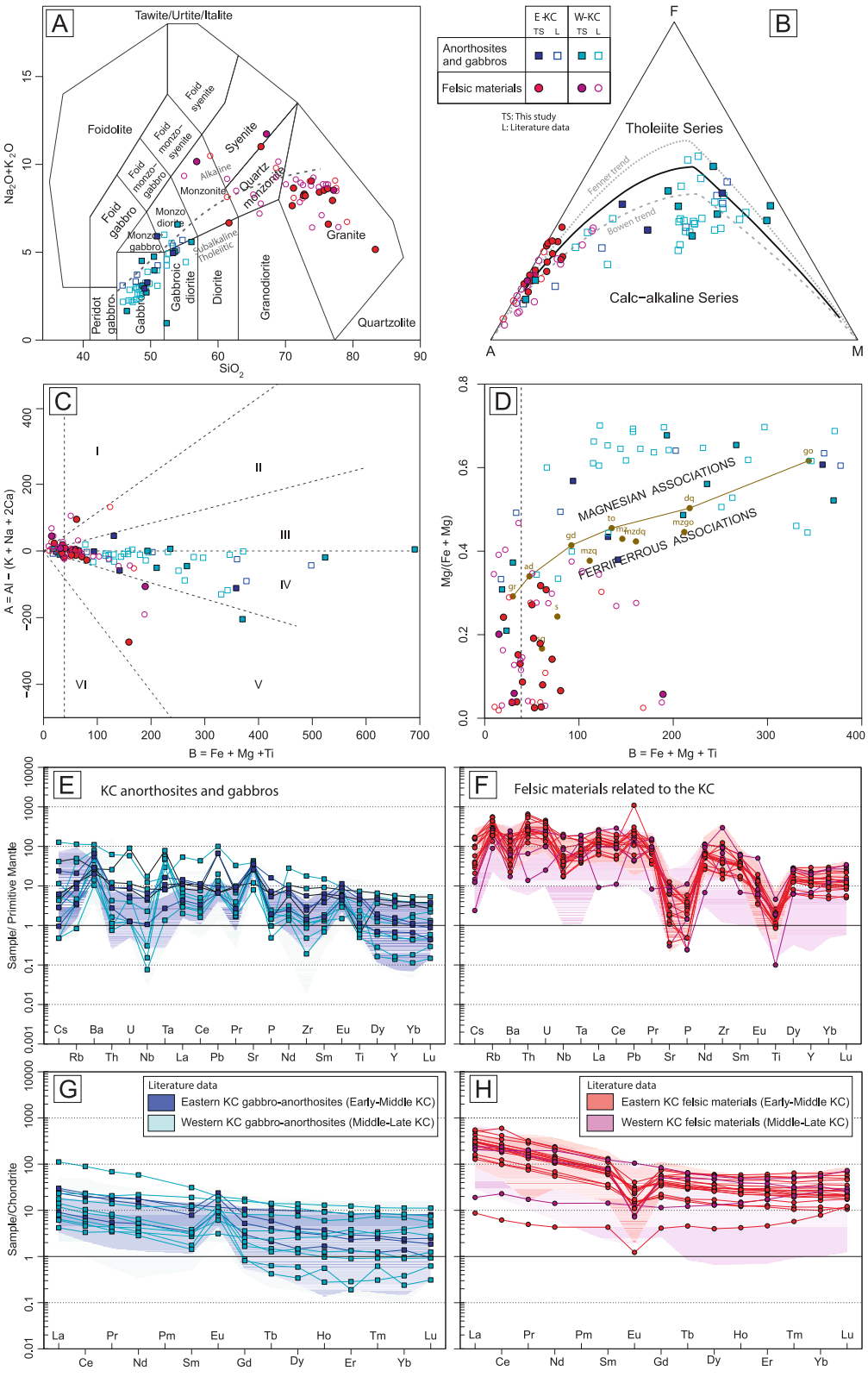

Fig. 3. Geochemical classification diagrams of the studied samples from the eastern KC segments (E-KC) and western KC areas (W-KC). A) TAS diagram of Middlemost (1994). Division of alkaline from sub-alkaline rock series (dotted grey line) from Irvine and Baragar (1971). B) AFM diagram, showing the boundary between tholeiitic and calc-alkaline igneous suites (black solid line) and the projection of Fenner (grey dotted line) and Bowen (grey dashed line) magma evolution trends of Vermeesch and Pease (2021). C) A-B diagram of Debon and Le Fort (1983). D) B vs. Mg/(Fe + Mg) diagram of Debon and Le Fort (1988). E, F) Spider plots normalized to Primitive Mantle of McDonough and Sun (1995). G, H) Chondrite-normalised REE diagram. Normalisation values are from Boynton (1984). Composition of KC gabbro-anorthosite and felsic materials of literature data taken from Baxe (2007), Kröner et al. (2015), Brower (2017), Kröner and Rojas-Agramonte (2017), and Milani et al. (2022).

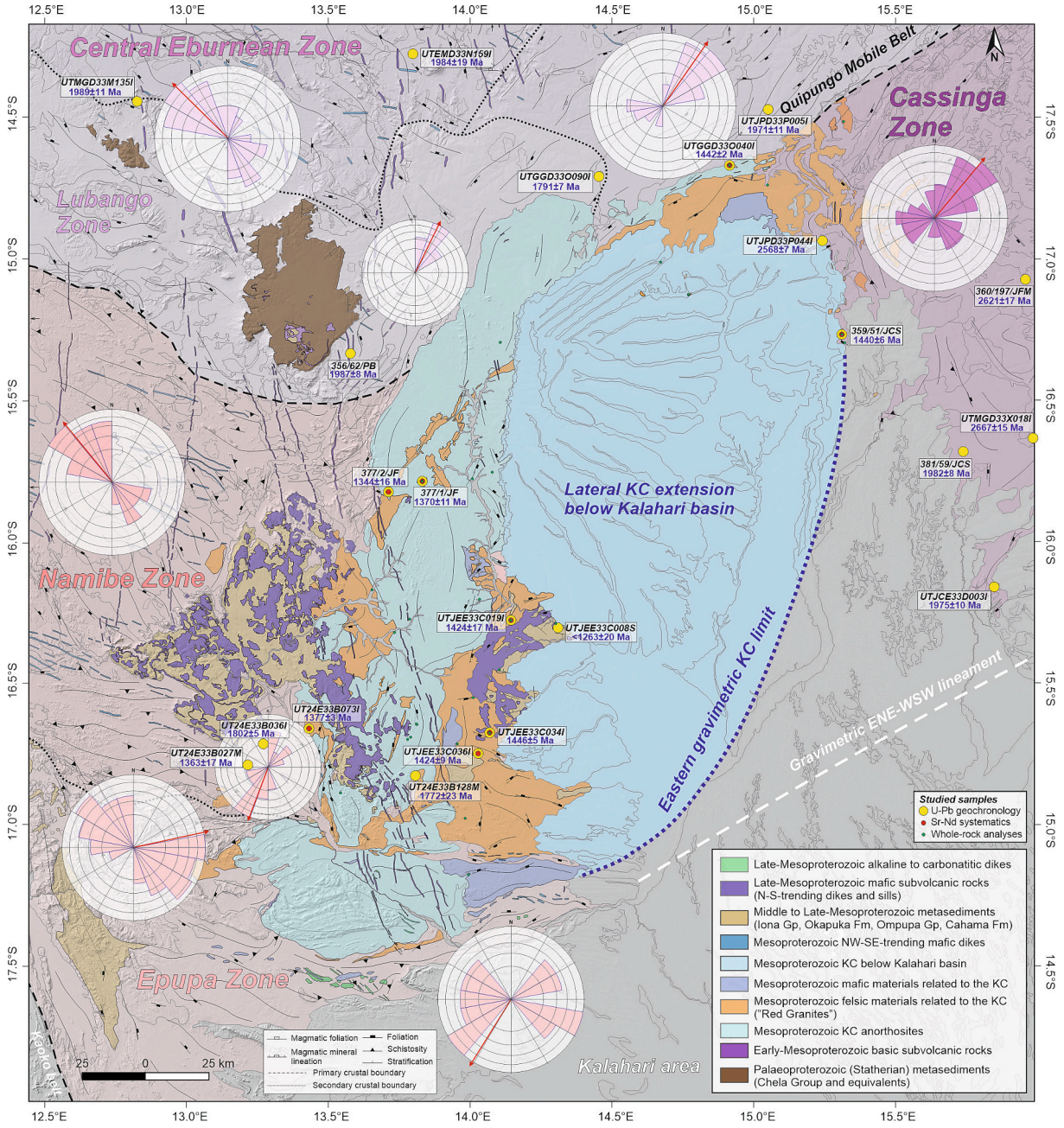

Fig. 4. Synthesised map of the studied zone showing the location of the studied samples and the main structural features discussed in the text. Rose diagrams of the Archaean to Mesoproterozoic materials are built by analysing the magmatic and metamorphic foliations projected in the map (according to those data from the PLANAGEO project and literature information). The crustal domains have been interpreted on the basis of the geochronological and structural analysis resumed in the main text, as well as the gravimetric information of Rey-Moral et al. (2022).

(MSWD = 1.10; upper intercept age) and 1986.5 ± 8.2 Ma (MSWD = 0.0005; concordia age), respectively (Fig. 5D-F).

A NE-SW trending granodiorite-gneiss (UTJPD33P005I) was sampled northeast of the KC (Fig. 4). In this area, the basement defines a linear NE-SW deformational zone, extending north-eastwards from the Quipungo region (Fig. S1). The sample shows a penetrative planar-linear metamorphic fabric, sub-parallel to the main NE-SW trending foliation and lineation of the country rock materials. Locally, it shows cataclastite-like deformational textures, suggesting brittle-ductile deformation. An upper intercept age of 1971 ± 11 Ma (MSWD = 0.37; Fig. 5G) was determined for the crystallisation age of the granodioritic protolith.

East of the KC, beyond the Kalahari sedimentary cover, distinct Palaeoproterozoic granitoid and volcanic-related felsic facies occur within the Archaean basement of the Cassinga Zone (Fig. 2). An undeformed medium- to coarse-grained biotite granite (381/59/JCS) and a NE-SW trending foliated granite (UTJCE33D003I) was sampled close to Cuvelai and 100 km north of Ondjiva, respectively (Fig. S1). These two samples provided U-Pb crystallisation ages of 1981.8 ± 7.5 Ma (MSWD = 0.003, concordia age; Fig. 5H) and 1975 ± 10 Ma (MSWD = 9.9, upper intercept age; Fig. 5I).

5.1.3. *Palaeoproterozoic Epupa-aged basement*

The Epupa-aged plutonic basement is represented by granitoid bodies, minor diorite to gabbroic rocks, and scarce ultrabasic materials, intrusive within the Eburnean basement and in the Namibe Group, further south (Fig. 4).

Samples UTGGD33O090I and UT24E33B036I consist of

Table 1
Summary of U-Pb geochronological results.

Sample	Lithology	Geological Unit	Coordinates		Age (Ma)	error (Ma)	Methodology
			Latitude	Longitude			
UTMGD33X018I	Foliated porphyritic granitoid	Archaean plutono-metamorphic basement	−15.597700	16.015067	2667	15	U-Pb TIMS IGME
360/197/JFM	Granite gneiss	Archaean plutono-metamorphic basement	−15.072267	15.985601	2621	17	U-Pb SHRIMP GEOLAB
UTJPD33P044I	Foliated granite	Archaean plutono-metamorphic basement	−14.938065	15.245468	2567.8	6.8	U-Pb SHRIMP IBERSIMS
UTMGD33M135I	Foliated porphyritic granite	Palaeoproterozoic plutono-metamorphic basement (Eburnean)	−14.445077	12.831390	1989	11	U-Pb SHRIMP IBERSIMS
356/62/PB	Bt granite gneiss	Palaeoproterozoic plutono-metamorphic basement (Eburnean)	−15.342279	13.577734	1988.6	9.5	U-Pb SHRIMP GEOLAB
UTEMD33N159I	Schlieric monzogranite	Palaeoproterozoic plutono-metamorphic basement (Eburnean)	−14.268835	13.798710	1984	19	U-Pb SHRIMP IBERSIMS
381/59/JCS	Granite	Palaeoproterozoic plutono-metamorphic basement (Eburnean)	−15.678479	15.760435	1981.8	7.5	U-Pb SHRIMP GEOLAB
UTJCE33D003I	Granite	Palaeoproterozoic plutono-metamorphic basement (Eburnean)	−16.138197	15.867944	1975	10	U-Pb TIMS IGME
UTJPD33P005I	Granite gneiss	Palaeoproterozoic plutono-metamorphic basement (Eburnean)	−14.435096	15.069294	1971	11	U-Pb SHRIMP IBERSIMS
UT24E33B036I	Diorite	Palaeoproterozoic igneous basement (Epupa)	−16.720789	13.267416	1801.8	4.6	U-Pb TIMS IGME
UTGGD33O090I	Gabbro	Palaeoproterozoic igneous basement (Epupa)	−14.697922	14.458075	1791.1	6.8	U-Pb TIMS IGME
UT24E33B128M	Amphibolite	Palaeoproterozoic Epupa Metamorphic Complex	−16.824506	13.811902	1772	23	U-Pb SHRIMP IBERSIMS
UTGGD33O040I	Anorthosite	Mesoproterozoic Kunene Complex	−14.661268	14.925023	1441.9	1.5	U-Pb TIMS IGME
UTJEE33C034I	Rhyodacite	Mesoproterozoic felsic intrusions related to the Kunene Complex	−16.670891	14.070312	1445.8	1.9	U-Pb TIMS IGME
UTJEE33C034I_rep	Rhyodacite	Mesoproterozoic felsic intrusions related to the Kunene Complex	−16.670891	14.070312	1449.7	7.7	U-Pb SHRIMP IBERSIMS
359/51/JCS	Granite porphyry	Mesoproterozoic felsic intrusions related to the Kunene Complex	−15,267009	15.319934	1440.1	5.6	U-Pb SHRIMP GEOLAB
UTJEE33C036I	Pinkish syenitic granite	Mesoproterozoic felsic intrusions related to the Kunene Complex	−16.753148	14.027514	1424	9	U-Pb TIMS IGME
UTJEE33C019I	Coarse-grained reddish granite	Mesoproterozoic felsic intrusions related to the Kunene Complex	−16.275356	14.145899	1423.7	9.3	U-Pb SHRIMP IBERSIMS
377/1/JF	Episyenite	Mesoproterozoic felsic intrusions related to the Kunene Complex	−15.784167	13.835556	1370	11	U-Pb SHRIMP GEOLAB
UT24E33B073I	Granodiorite	Mesoproterozoic felsic intrusions related to the Kunene Complex	−16.666660	13.430350	1377.4	5.8	U-Pb TIMS IGME
UT24E33B027M	Basalt dike	Mesoproterozoic basic magmatism related to the Kunene Complex	−16.784726	13.209454	1363	17	U-Pb SHRIMP IBERSIMS
377/2/JF	Anorthosite	Mesoproterozoic Kunene Complex	−15.826389	13.714444	1344	16	U-Pb SHRIMP GEOLAB
UTJEE33C008S	Microconglomeratic sandstone	Cahama Formation	−16.291600	14.309900	1263	20	U-Pb SHRIMP IBERSIMS

intermediate to basic plutonic rocks (Fig. S1). Sample UTGGD33O090I is an undeformed gabbro intrusive into the Eburnean basement north of the KC. Four zircon fractions, anchored by a concordant analysis, display a co-linear discordancy pattern with a U-Pb upper intercept age of 1791.1 ± 6.8 Ma (MSWD = 0.37; Fig. 5J), interpreted as the emplacement age of the gabbro. Sample UT24E33B036I is a medium-grained quartz-diorite located southwest of the KC. The quartz-diorite shows a NW-SE hornblende-defined lineation sub-parallel to the crenulation lineation and fold axes found in the nearby metamorphic basement (Potti et al., 2021). The U-Pb analyses of this sample provide a crystallisation age of 1801.8 ± 4.6 Ma (MSWD = 0.34; Fig. 5K), determined by the co-linear regression line of four zircon fractions.

A basic amphibolite (sample UT24E33B128M) was sampled in the southern region of the Angolan KC (Fig. 4). In this area, the Epupa-aged basement forms a narrow, elongate N-S trending body sandwiched between the Mesoproterozoic anorthositic and granitic rocks of the KC. This metabasic rock shows a plano-linear gneissic fabric, overprinted by folding and crenulation that resulted in the formation of tight isoclinal folds. These structures indicate a complex deformational overprint of the Epupa intrusives in this sector. U-Pb analyses define an upper intercept age of 1772 ± 23 Ma (MSWD = 1.09; Fig. 5L), reflecting the emplacement age of the mafic protolith.

5.2. Kunene Complex

5.2.1. Mesoproterozoic KC anorthosites and basic rocks

We sampled two anorthosites from the northern (UTGGD33O040I) and central (377/2/JF) parts of the Kunene Complex, along with a basaltic dike (UT24E33B027M) intrusive into the Namibe Group SW of the KC (Fig. 4).

Sample UTGGD33O040I was collected from the northeasternmost edge of the KC, near Matala, and exhibits a whitish colour due to pervasive hydrothermal alteration (Fig. S1). Five zircon fractions from this sample define a co-linear regression line with an upper intercept age of 1441.9 ± 1.5 Ma (MSWD = 1.9; Fig. 6A), identical to the $^{207}Pb/^{206}Pb$ weighted mean age (1441.3 ± 1.2 Ma, MSWD = 1.6). This sample displays a $^{87}Sr/^{86}Sr_{(i)}$ value of 0.708629, an $\varepsilon Nd_{(i)}$ of −2.2, and a T_{DM2} age of 2.09 Ga (Table 2).

Sample 377/02/JF is a medium- to coarse-grained anorthosite collected west of the central part of the KC, near Pocolo (Fig. S1). It lacks foliation and shows no signs of deformation and recrystallisation. This sample provides a U-Pb crystallisation age of 1344 ± 16 Ma (MSWD = 0.0011; concordia age; Fig. 6B), a $^{87}Sr/^{86}Sr_{(i)}$ value of 0.703454, an $\varepsilon Nd_{(i)}$ of + 0.1, and a T_{DM2} age of 1.84 Ga (Table 2).

Sample UT24E33B027M is an undeformed NW-SE trending dolerite dike intrusive into the Namibe Group, southwest of the KC. Only four zircon grains were extracted from this sample. The analysed zircons

Table 2
Sm-Nd and Rb-Sr composition of the studied Mesoproterozoic KC rocks.

Sample	Lithology	Coordinates		Age (Ma)	Sm (ppm)	Nd (ppm)	$^{147}Sm/^{144}Nd$	error	$^{143}Nd/^{144}Nd$	error	$\varepsilon Nd_{(i)}$	T_{DM2}	Rb (ppm)	Sr (ppm)	$^{87}Rb/^{86}Sr$	error	$^{87}Sr/^{86}Sr$	error	$^{87}Sr/^{86}Sr_{(i)}$
		Latitude	Longitude																
UTGGD33O040I	Anorthosite	−14.661268	14.925023	1442	2.08	10.70	0.117537	0.004987	0.5117763	0.000001	−2.2	2.09	12.60	709.90	0.051355	0.002179	0.709692	0.000003	0.708629
377/02/JF	Anorthosite	−15.826389	13.714444	1344	0.70	3.49	0.121817	0.000716	0.5119810	0.000006	0.1	1.84	4.00	493.00	0.023463	0.000995	0.703906	0.000021	0.703454
377/01/JF	Episyenite	−15.784167	13.835556	1378	23.55	116.20	0.122542	0.000724	0.5119005	0.000005	−1.3	1.97	53.50	147.50	1.050965	0.044589	0.724203	0.000022	0.703435
359/51/JCS	Granite porphyry	−15.267009	15.319934	1440	15.74	90.13	0.105581	0.000625	0.5115476	0.000005	−4.5	2.25	223.90	43.80	15.175237	0.643831	0.975465	0.000018	0.661968*
UTJEE33C019I	Granite	−16.275356	14.145899	1424	14.05	83.10	0.102228	0.004337	0.5115089	0.000001	−4.8	2.26	158.20	21.20	22.345360	0.948033	1.066711	0.000005	0.610270*
UTJEE33C034I	Rhyodacite	−16.670891	14.070312	1450	13.42	77.60	0.104565	0.004436	0.5112843	0.000001	−9.3	2.60	113.10	128.30	2.562906	0.108735	0.758922	0.000003	0.705605

* *Post-crystallization disturbance of the Rb-Sr system.*

yield two Palaeoproterozoic (Eburnean) and two Mesoproterozoic (sub) concordant dates (Fig. 6C). Despite de irregular CL structures observed in the younger Mesoproterozoic zircon crystal (analysis 3.1; Fig. S5), the Th/U ratio of 0.67 would be consistent with partial recrystallisation occurring during the final stages of magma crystallisation. Hence, the 1363 ± 17 Ma (MSWD = 1.3) concordia age of the younger Mesoproterozoic zircon is interpreted as the best estimate for the crystallisation age of this sample, similar to the age reported for other WNW-trending dikes intruding into the Namibe Group (Fig. 2; 1385 ± 5 Ma; Ernst et al., 2014).

5.2.2. *Mesoproterozoic KC felsic rocks*

Four granitoids (samples UTJEE33C019I, UTJEE33C036I, 377/1/JF and UT24E33B073I) and two felsic subvolcanic rocks (samples 359/51/JC and UTJEE33C034I) were collected from several locations across the KC (Fig. 4). Notably, four of these samples come from regions where the felsic magmatism associated with the KC has not previously been dated.

Sample 359/51/JC is a granite porphyry forming a N-S directed outcrop exposed along the Cunene river, surrounded by the Cenozoic sediments of the Kalahari Group. The concordia age of 1440.1 ± 5.6 Ma (MSWD = 1.8; Fig. 6D) is interpreted as the crystallisation age of this sample. This age overlaps within uncertainty with that obtained for the anorthosite dated in the same region (sample UTGGD33O040I, 1441.9 ± 1.5 Ma; Fig. 6A). This sample shows an $\varepsilon Nd_{(i)}$ value of −4.5 and a T_{DM2} age of 2.25 Ga; the $^{87}Sr/^{86}Sr_{(i)}$ value of 0.661968, lower than the BABI, indicates post-recrystallisation disturbance of the Rb-Sr system (Table 2).

Two granitoids (UTJEE33C019I and UTJEE33C036I) were collected near and south of Cahama. These rocks are coarse-grained syenogranites, occasionally displaying a slight sub-vertical planar magmatic foliation and a preferred mineral orientation in a NE-SW to ENE-WSW direction (Fig. S1). They contain sub-rectangular and ovoid enclaves of porphyritic felsic volcanic rocks. Both samples reveal identical U-Pb crystallisation ages of 1424 ± 17 Ma (MSWD = 0.53, upper intercept age; Fig. 6E) and 1423.7 ± 9.3 Ma (MSWD = 0.74, concordia age; Fig. 6F). Granitoid UTJEE33C019I displays an $\varepsilon Nd_{(i)}$ value of −4.8 and a T_{DM2} age of 2.26 Ga; the $^{87}Sr/^{86}Sr_{(i)}$ value of 0.610270, lower than the BABI, indicates post-recrystallisation disturbance of the Rb-Sr system (Table 2).

A rhyodacite (UTJEE33C034I) was collected ca. 10 km NNE of granite UTJEE33C036I (Fig. S1). This rhyodacite has a massive appearance with an inequigranular to porphyritic texture. Four zircon fractions were analysed by ID-TIMS; however, two of these fractions contain very high common Pb content, providing unreliable results. The other two fractions define a discordia line with an upper intercept age of 2447 ± 52 Ma and a lower intercept age of 1445.6 ± 5.4 Ma (MSWD = 1.3; Fig. 6G). The older age indicates inherited zircon incorporated from the underlying basement, while the younger age is anchored on a concordant zircon fraction that provides a concordia age of 1445.8 ± 1.9 Ma (MSWD = 0.0035), interpreted as the extrusion age of the rhyodacite. Since this age was derived from a single fraction, we have analysed zircons from the same sample by U-Pb SHRIMP. Ten of the sixteen analysed zircon yield a concordia age of 1449.7 ± 7.7 Ma (inset of Fig. 6G), which is consistent within uncertainty with the ID-TIMS age, thereby validating the 1445.8 ± 1.9 Ma age as the best estimate for the crystallisation of the rhyodacite. The rhyodacite age aligns with the presence of felsic volcanic enclaves in the nearby ca. 1424 Ma red granites. The rhyodacite exhibits a $^{87}Sr/^{86}Sr_{(i)}$ value of 0.705605, an $\varepsilon Nd_{(i)}$ value of −4.8 and a T_{DM2} age of 2.26 Ga (Table 2).

Two additional granitoids were sampled from the central- and southwestern parts of the KC. Sample 377/1/JF is an episyenite collected near Pocolo, exhibiting intense deformation along a prominent NE-SW fault structure. A concordia age from six zircon U-Pb data of 1370 ± 11 Ma (MSWD = 0.75) is interpreted as the crystallisation age of the protolith, which is similar to the upper intercept age of 1375 ± 18 Ma (MSWD = 0.18; Fig. 6H). This sample shows a $^{87}Sr/^{86}Sr_{(i)}$ value of

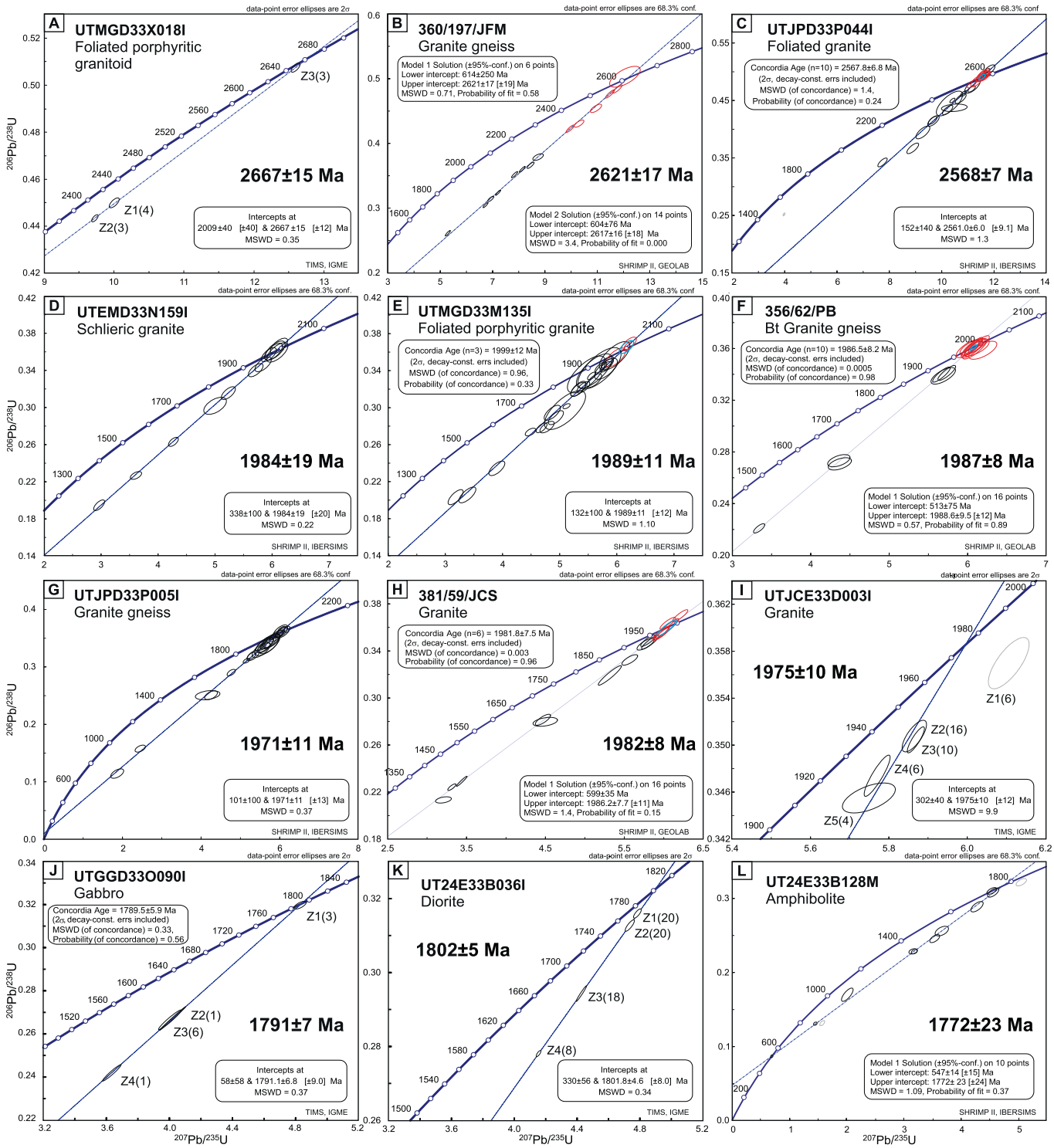

Fig. 5. U-Pb concordia diagrams obtained of the studied Archaean to Palaeoproterozoic samples via SHRIMP tools at (A, E, G) the GEOLAB laboratories of São Paulo (Brazil) and (B, C, D, F, K) the IBERSIMS laboratories of Granada (Spain), and via U-Pb CA-ID-TIMS (H, I, J) at the IGME laboratories of Madrid (Spain). (A) Sample UTMGD33X018I (porphyritic granite-gneiss), 2621 ± 17 Ma. (B) Sample 360/197/JFM (gneissic granite), 2621 ± 17 Ma. (C) Sample UTJPD33P044I (foliated porphyritic granite), 2568 ± 7 Ma. (D) Sample UTEMD33N159I (schlieric granite), 1984 ± 19 Ma. (E) Sample UTMGD33M135I (foliated porphyritic granite), 1989 ± 11 Ma. (F) Sample 356/62/PB (granite gneiss), 1982 ± 8 Ma. (G) Sample UTJPD33P005I (granite gneiss), 1971 ± 11 Ma. (H) Sample 381/59/JCS (isotropic granite), 1982 ± 8 Ma. (I) Sample UTJCE33D003I (slightly foliated granite), 1975 ± 10 Ma. (J) Sample UTGGD33O090I (unfoliated gabbro), 1791 ± 7 Ma. (K) Sample UT24E33B036I (foliated quartz-diorite), 1802 ± 5 Ma. (L) Sample UT24E33B128M (amphibolite), 1772 ± 23 Ma. Error ellipses of SHRIMP data are at 68.3 % confidence, whereas those of TIMS are plotted at 2σ level.

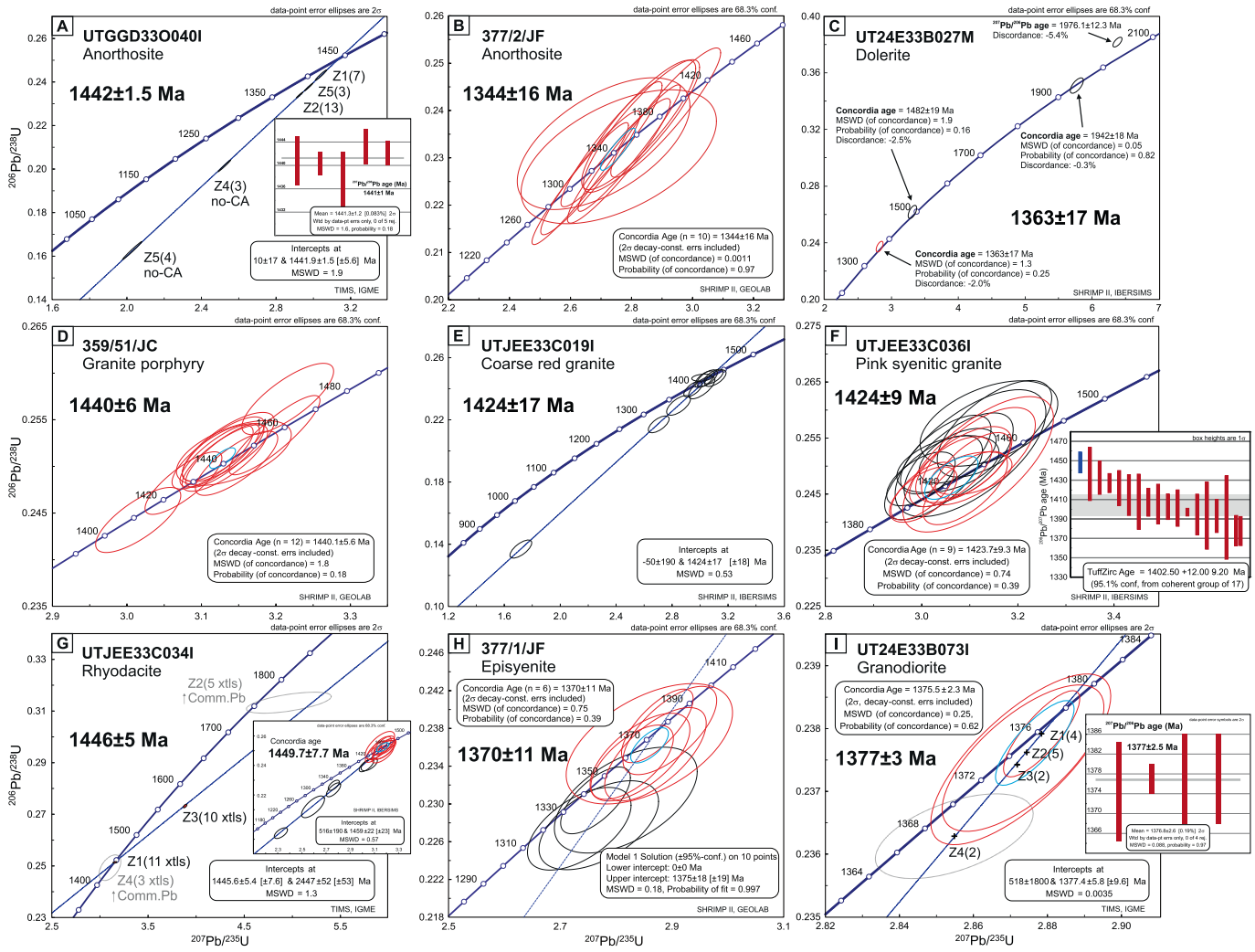

Fig. 6. U-Pb concordia diagrams of the studied Mesoproterozoic samples obtained via U-Pb CA-ID-TIMS (A, G, I) at the IGME laboratories of Madrid (Spain), and via U-Pb SHRIMP IIe tools at (B, D, H, inset of G) the GEOLAB laboratories of São Paulo (Brazil) and at (C, E, F) the IBERSIMS laboratories (Granada, Spain). (A) Sample UTGGD33O040I (hidrothermalised anorthosite), 1442 ± 2 Ma. (B) Sample 377/2/JF (anorthosite), 1344 ± 16 Ma. (C) Sample UT24E33B027M (dolerite dike), 1363 ± 17 Ma. (D) Sample 359/51/JC (granite porphyry), 1440 ± 6 Ma. (E) Sample UTJEE33C019I (coarse-grained red granite), 1424 ± 17 Ma. (F) Sample UTJEE33C036I (syenogranite), 1424 ± 9 Ma. (G) Sample UTJEE33C034I (rhyodacite), 1446 ± 5 Ma (TIMS). SHRIMP concordia age of 1450 ± 8 Ma (inset). (H) Sample 377/1/JF (episyenite), 1370 ± 11 Ma. (I) Sample UT24E33B073I (granodiorite), 1377 ± 3 Ma. Error ellipses of SHRIMP data are at 68.3 % confidence, whereas those of TIMS are plotted at 2σ level.

0.703435, an $\varepsilon Nd_{(i)}$ value of −1.3 and a T_{DM2} age of 1.97 Ga (Table 2). Sample UT24E33B073I is a medium-grained granodiorite with a weak, NNW-SSE to N-S oriented, sub-vertical, planar magmatic foliation. This granodiorite includes orthoderived enclaves. The sample reveals a concordia age of 1375.5 ± 2.3 Ma (MSWD = 0.25; Fig. 6I), obtained from three zircon fractions, showing an upper intersection of 1377.4 ± 5.8 Ma (MSWD = 0.0035). The $^{207}Pb/^{206}Pb$ weighted mean age of 1376.8 ± 2.6 Ma (MSWD = 0.09; Fig. 6I), obtained from the four analysed zircon fractions, is interpreted as the crystallisation age of the granodiorite.

5.3. Kunene Complex sedimentary cover

In the Cahama region, a ca. 80 to 100 m thick, undeformed, medium- to coarse-grained, light yellowish to pinkish coloured siliciclastic sequence, discordantly overlies the KC (Fig. 4). Fragments of red granites are locally observed in conglomeratic levels (Carvalho et al., 1987; Escuder-Viruete and Gumiel, 2021). This siliciclastic sequence is intruded by undeformed mafic sills and dikes. A coarse-grained sandstone (sample UTJEE33C008S) was selected for U-Pb geochronology (Fig. S1). The 51 subconcordant/concordant detrital zircon analyses display a Kernell density estimate (KDE) distribution of $^{207}Pb/^{206}Pb$ ages ranging from 3.0 to 1.17 Ga (Fig. 7). The age distribution reveals an Archaean contribution with ages of 3.0 Ga and 2.7–2.6 Ga (10 %), a small 2.15 Ga fraction (7 %), and significant Eburnean (2.05–1.95 Ga; 18 %) and Epupa (1.82–1.78 Ga; 37 %) components. Minor ca. 1.5 Ga zircon are present, along with significant 1.4–1.25 Ga zircon (27 %) derived from the underlying Kunene Complex and other late-Mesoproterozoic materials. The youngest component, reaching 1.17 Ga, shows a large analytical error and is subconcordant, rendering it unreliable. Therefore, the most robust estimate for the maximum depositional age of the sandstone is provided by a cluster of three concordant analyses with a concordia age of 1263 ± 20 Ma (MSWD = 0.43; Fig. 7).

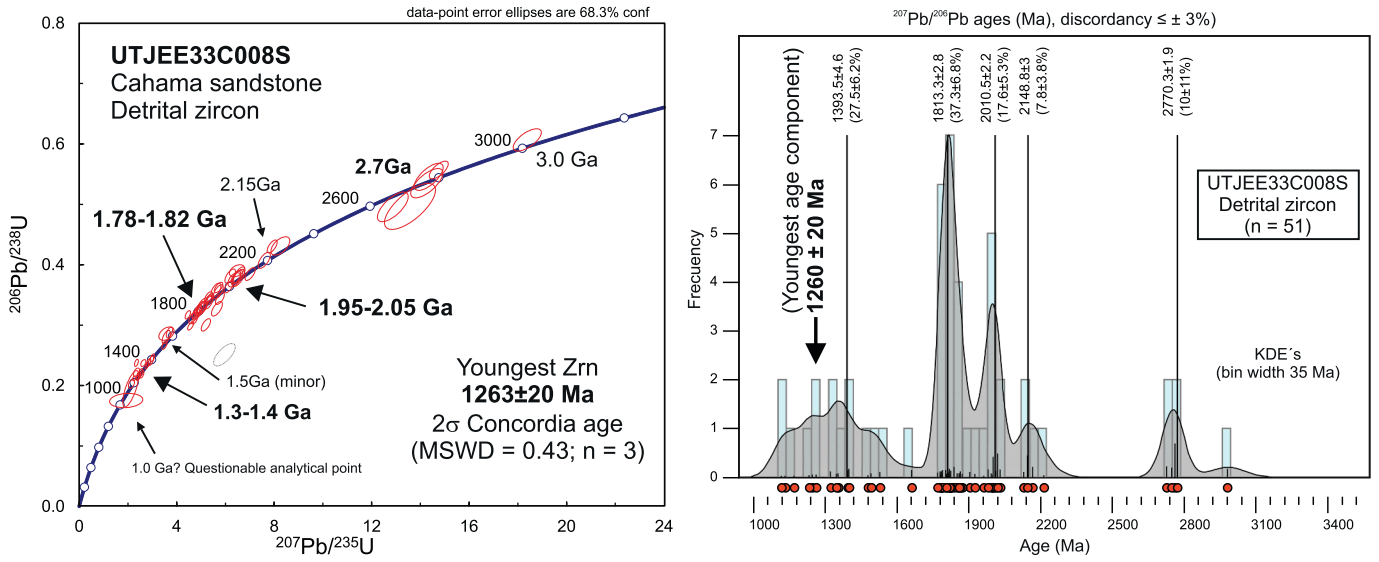

Fig. 7. U-Pb concordia diagram and KDE histogram for the siliciclastic sample from the Cahama region (sample UTJEE33C008S). On the left are shown the concordia plots and calculated concordia ages for the maximum depositional age of the Cahama sequence. Error ellipses are shown at 68.3 % confidence. On the right, the probability density plot of the detrital zircon U-Pb ages of the Cahama sandstone shows the main intervals of zircon populations. The most probable maximum depositional age of this sedimentary sample is constrained in 1263 ± 20 Ma, using the most-concordant U-Pb results of the youngest zircon populations.

6. Discussion

6.1. Age distribution and crustal framework of the Archaean to Palaeoproterozoic basement

Several studies have proposed the existence of various tectonic domains within the Angolan Shield (Carvalho et al., 2000; McCourt et al., 2013; Jelsma et al., 2018): Kwanza Horst, Central Shield Zone, Cassinga Zone, Central Eburnean Zone and Lubango Zone (Fig. 1). Building upon this framework, a combined analysis of the available gravimetric and magnetic response of the SW Angolan Shield (Figs. 8, 9; Rey-Moral et al., 2022; Mochales et al., 2025), together with geological, structural, and geochronological data, has contributed to a redefinition of the crustal architecture surrounding the KC (Fig. 10): Cassinga Zone, Central Eburnean Zone, Lubango Zone, Namibe Zone, Epupa Zone, and the Kalahari Area (Rodrigues et al., 2021; Merino-Martínez et al., 2022). These contrasting crustal domains significantly influenced the generation and emplacement of the Kunene Complex during the Mesoproterozoic. The key features of each crustal zone are outlined below.

Cassinga Zone: the eastern boundary of the KC

The Cassinga Zone, located east of the KC (Fig. 4), is composed of Neoarchaean to Palaeoproterozoic (Eburnean) igneous and metamorphic materials showing U-Pb crystallisation ages ranging from 2666 to 2568 Ma (Fig. 5A-C) and from 1982 to 1971 Ma (Fig. 5G-I). The low to extremely low gravimetric values characteristic of the Cassinga Zone agree with the existence of an ancient crust (Fig. 8; Rey-Moral et al., 2022). Positive magnetic anomalies with NNE-SSW to NE-SW magnetic trends characterised this region (Fig. 9; Mochales et al., 2025). The presence of both Neoarchaean and Eburnean granitoids intruding the Jamba Group supports previous suggestions that this *meta*-volcanosedimentary sequence represents an Archaean greenstone belt (e.g., Korpershoek, 1970, 1984; Carvalho and Alves, 1993; Machado et al., 1996; Silva, 2005). Importantly, no evidence of younger Epupa-aged materials has been identified in this region.

Central Eburnean Zone and Lubango Zone: the northwestern boundaries of the KC

The Central Eburnean Zone (CEZ) and the Lubango Zone (LZ) form the northwestern boundary of the KC and are characterised by a complex Palaeoproterozoic crust dominated by Eburnean-aged gneissic-granitic-migmatitic rocks dated between 2038 ± 28 and 1947 ± 5 Ma (Figs. 2, 5D-G, 10; Pereira et al., 2011, 2013; McCourt et al., 2013; Milani et al., 2022). The southern portion of the CEZ, the Lubango Zone, is intruded by Epupa-aged (ultra-)mafic to felsic magmatic bodies dated between 1844 ± 20 and 1744 ± 16 Ma (Figs. 5J, 10; Delor et al., 2006; Jelsma et al., 2011, 2018; Pereira et al., 2011, 2013; McCourt et al., 2013; Milani et al., 2022; Campeny et al., 2023). The high to medium gravity responses and NW-SE magnetic lineaments that characterise these zones transition to medium to low gravity values and NE-SW trending directions adjacent to the Quipungo belt and the Kunene Complex (Figs. 8, 9; Rey-Moral et al., 2022; Mochales et al., 2025). The presence of Meso- to Neoarchaean Hf and Nd model ages in both Eburnean and Epupa-aged granitoids within the CEZ and LZ provides compelling evidence for the existence of an underlying Archaean crust (Fig. 8; Pereira et al., 2011, 2013; Milani et al., 2022).

Namibe and Epupa Zones: western and southwestern boundaries of the KC

Geochronological data indicate that the Namibe and Epupa zones, previously included within the Lubango Zone (Carvalho et al., 2000), are primarily composed of Epupa-aged materials, with U-Pb ages ranging from 1861 ± 3 Ma to 1739 ± 9 Ma (Figs. 2, 5K, 5L; e.g., Kröner et al., 2004, 2010, 2015; Gonçalves, 2010; Lehmann et al, 2020). This is further supported by the large set of whole-rock Rb-Sr ages published for the Namibe Zone, clustering around 1882–1797 Ma (Fig. 10; Torquato and Allsopp, 1973; Torquato, 1974, 1977). The granitoids and orthogneisses of the Namibe and Epupa zones exhibit slightly subchondritic to suprachondritic Hf and Nd isotopic compositions (Kröner et al., 2010, 2015; Luft et al., 2011; Milani et al., 2022; Ferreira et al., 2024), corresponding to an average decrease of ca. 700 to 600 Ma in T_{DM2} ages relative to the Central Eburnean Zone (Fig. 8). This, coupled with the absence of exposed Eburnean-aged or older magmatic rocks, suggests that the underlying crust of the Namibe and Epupa zones is distinct from that of the Central Eburnean Zone (Kröner et al., 2010, 2015; Ferreira et al., 2024). Moreover, the high to medium gravimetric signatures displayed by these zones indicate a younger and thinner crust compared to the gravimetric response of the Cassinga Zone (Fig. 8; Rey-Moral et al., 2022). The WNW-ESE to NW-SE magnetic lineaments featuring this zone also shift towards NE-SW orientations towards the Kunene Complex (Fig. 9; Mochales et al., 2025).

It should be noted that a WNW-ESE trending tectonic contact separating the Angolan and Namibian KC and country rocks has been

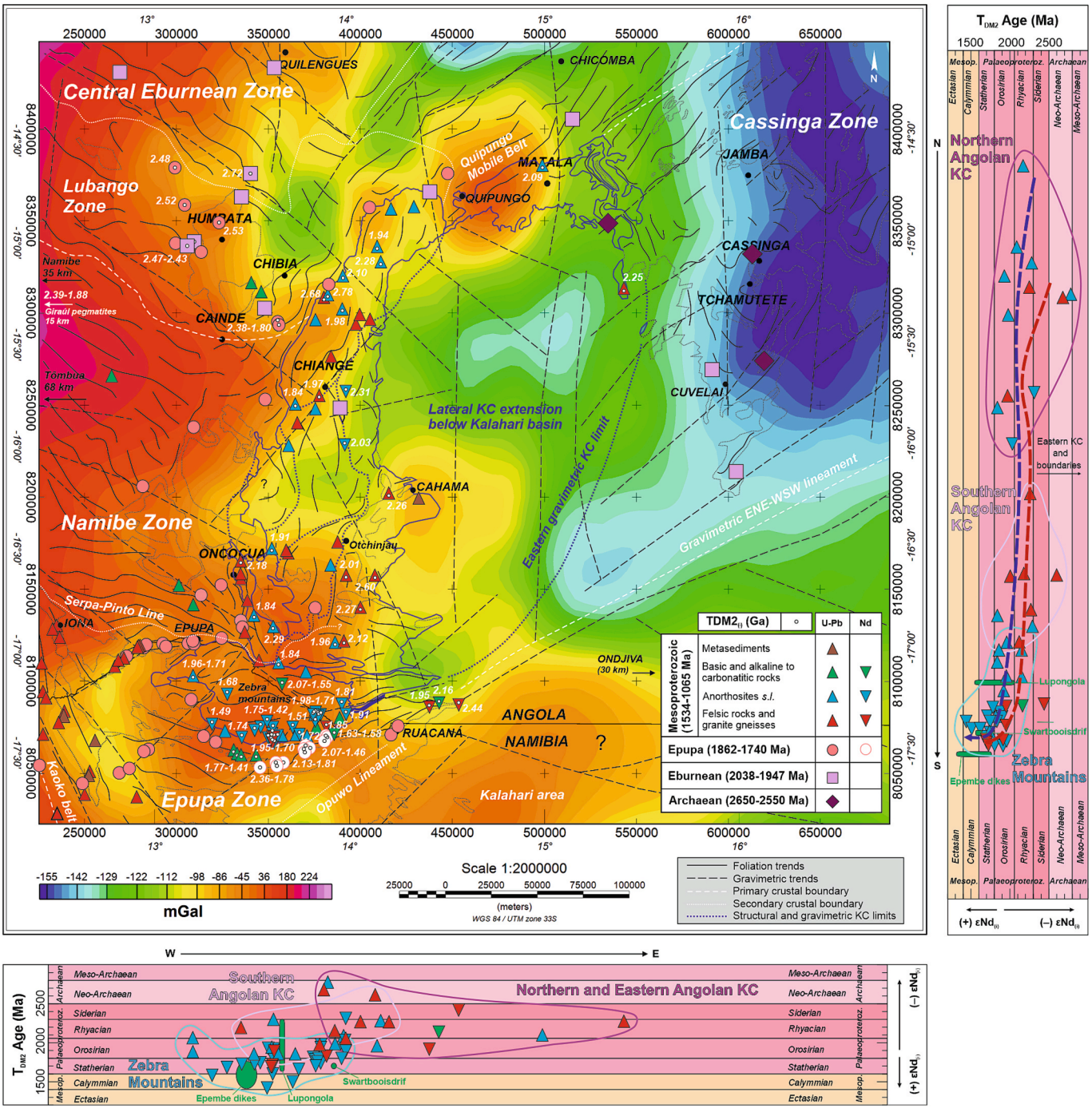

Fig. 8. Bouguer anomaly map of the studied area (modified from Rey-Moral et al., 2022), showing the contrasted crustal domains described in the text. The limit of the outcropping KC is shown in blue thick line, whereas the deduced eastern extension of the KC, below the Kalahari cover, is shown in blue dashed line. Thin dotted black lines delineate the main Archaean to Proterozoic (meta-) volcano-sedimentary sequences described in the text. The U-Pb geochronological data are projected grouped into the main tectono-thermal events (see legend inset), showing the calculated depleted model ages (T_{DM2}; in Ga) of those samples with available Sm-Nd isotope composition. The calculated T_{DM2} of Mesoproterozoic materials are shown on a vertical transect from N to S (right) and from W to E (down).

previously identified in this area (i.e., the Serpa Pinto Line; Vermaak, 1981; Carvalho and Alves, 1990; Lehmann et al., 2023). This structure aligns with the gravimetric, magnetic and structural variations observed between the Namibe and Epupa zones (Figs. 8-10), which we interpret as a potential lithospheric discontinuity or a secondary structural boundary between these crustal zones.

The Kalahari area: the southeastern boundary of the KC

The nature of the basement occurring southeast of the KC beneath the Cenozoic sediments, the Kalahari area, remains uncertain. Nevertheless, it is presumed to be equivalent to the Epupa Metamorphic Complex, similar to that found in the Eastern Kaoko Zone and the basement of the Northern Platform Zone of the Damara Domain (Corner and Durrheim, 2018). Indeed, Kröner et al. (2015) reported 1778 ± 4 Ma and 1775 ± 1 Ma U-Pb zircon crystallisation ages for a granite and an augen-gneiss from the Ruacana falls of NW Namibia (Fig. 2), suggesting that Epupa-aged materials composed the basement of this region. The most remarkable feature of this area is the important gravimetric ENE-WSW lineament that demarcates the boundary

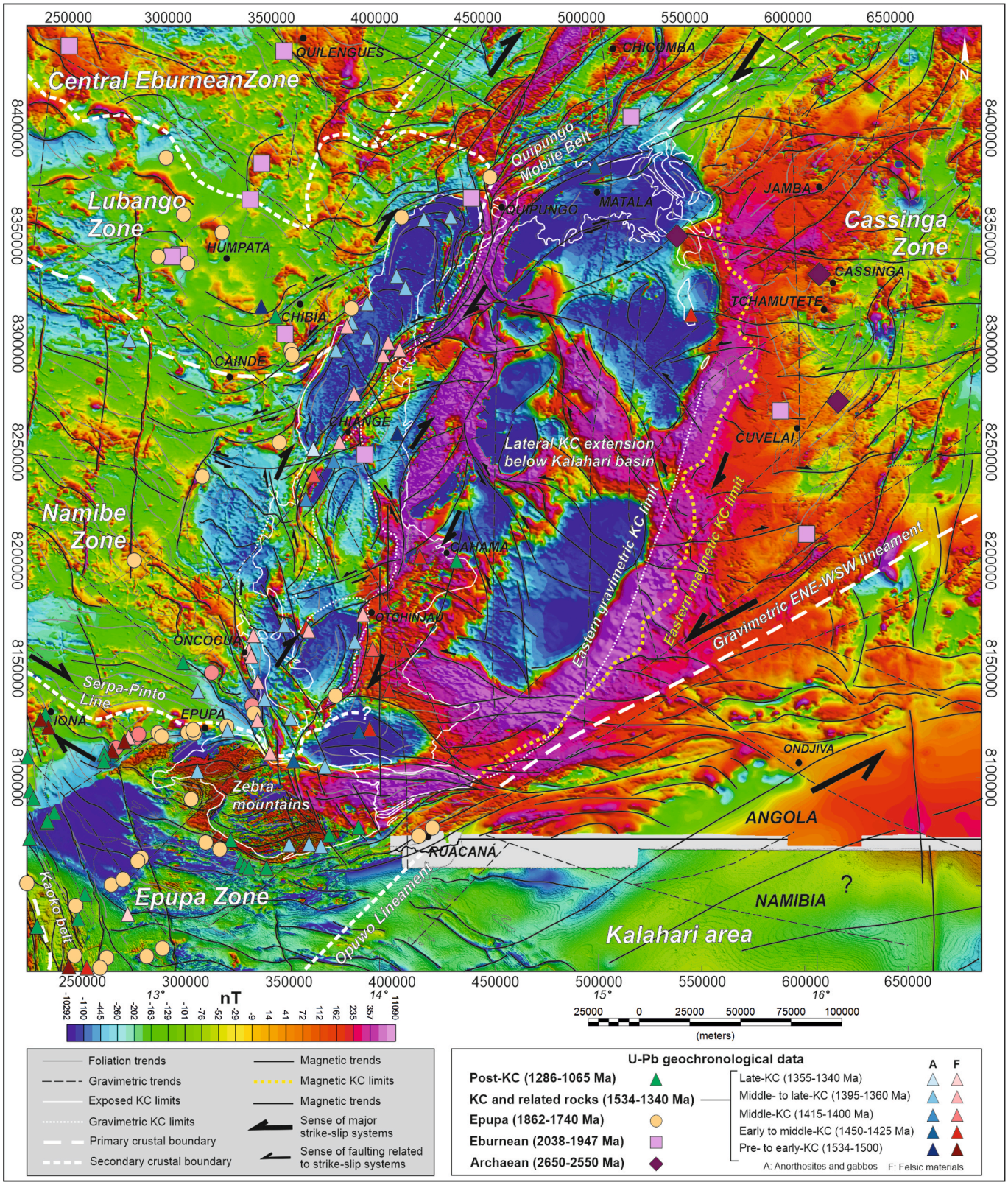

Fig. 9. Aeromagnetic (Total Magnetic Intensity Field – TMI) map of the studied region showing the structural information and kinematic criteria interpreted from the magnetic derivatives of basement and KC materials (modified from Mochales et al., 2025). It is also projected the U-Pb geochronological data of basement and KC materials (gabbro-anorthosites and felsic materials), classified according to the corresponding event and/or tectono-magmatic episode.

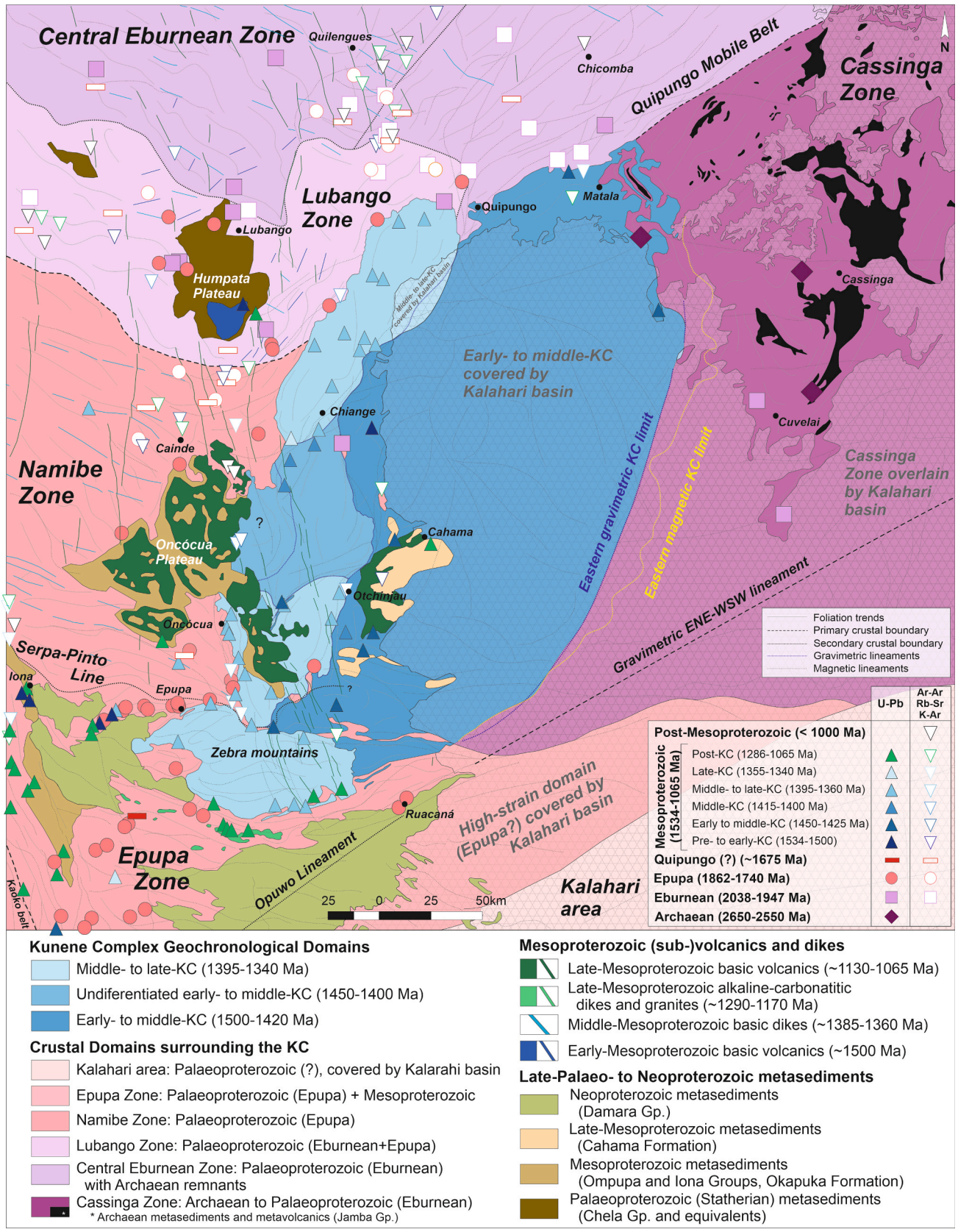

Fig. 10. Sketch map of the distinct crustal domains from the SW part of Angola and NW Namibia, and the geochronological domains proposed for the Kunene Complex, according to the published U-Pb data and the geological works from the PLANAGEO project. U-Pb geochronological results are compiled from the literature cited in the text and that obtained in this work. It is also projected the Ar-Ar plateau ages and the K-Ar and Rb-Sr isotope ages available in this region.

between the Cassinga Zone and a younger and thinner crust occurring southwards (Fig. 8; Rey-Moral et al., 2022). The magnetic lineaments indicate that significant tectonic processes have affected this boundary, resulting in the formation of contractional duplex structures associated with a large ENE-WSW trending left-lateral strike-slip system (Fig. 9).

6.1.1. Role of crustal anisotropy in the emplacement of the Kunene Complex

The structural and geophysical data indicate that the pre-existing crustal anisotropies played a significant role in the emplacement of the KC. The structural measurements obtained during PLANAGEO's geological mapping indicates contrasting NW-SE to NE-SW foliation trends between the basement to the west and east of the KC, respectively (Fig. 4; Rodrigues et al., 2021; Merino-Martínez et al., 2022). Nonetheless, these patterns are clearly disturbed near the Kunene Complex, adopting a structure almost parallel to the contact (Figs. 9, 10). Indeed, high-strain deformational fabrics suggest significant tectono-magmatic reworking of the basement during the intrusion of the KC (Fig. S1). In the Lubango area, the isotropic Epupa-aged leucogranites locally display NNE-trending steeply-dipping ductile fabrics parallel to the boundary of the KC (Merino-Martínez, 2022; Merino-Martínez and Goicoechea, 2022). Brittle-ductile NNE-SSW fabrics are also superimposed on the main WNW-ESE-trending gneissic foliations in the southwestern part of the complex (e.g., Lehmann et al., 2020; this work).

The contrasting geophysical features of the Palaeoproterozoic basement west of the KC (Central Eburnean and Namibe Zones) and the Archaean to Palaeoproterozoic crust to the east (Cassinga Zone), are separated by the regional NNE-SSW trend of the KC (Fig. 8; Rey-Moral et al., 2022; Mochales et al., 2025). This trend aligns with the NE-SW trending Quipungo Mobile Belt, which is assumed to have formed and stabilised between 1800 and 1650 Ma (e.g., Silva et al., 1973; Torquato et al., 1979). A large NNE-SSW dextral strike-slip system is outlined by the magnetic lineaments, suggesting the Quipungo Belt represents a high-strain deformational zone (Fig. 9). In fact, the occurrence of a series of thermal resetting events in the basement NW and SW of the KC, as evidenced by both Rb-Sr and U-Pb data constrained between 1700 and 1550 Ma (Fig. 10; Mendes, 1968; Torquato et al., 1979; Carvalho and Tassinari, 1992; Milani et al., 2022), points to tectono-thermal activity linked to the crustal structuring from late-Statherian to Calymmian times. Therefore, the Quipungo Belt likely represents a major structural weakness zone that facilitated crustal instability, fracturing processes, and pathways for KC magmatism.

On the other hand, the macrostructural elongation and geophysical signatures of the southern KC bodies and the Epupa basement overlap with the E-W direction of the Serpa-Pinto Line (Figs. 4, 9; Fig. S1). The nature of this structure remains uncertain. It might represent: i) an inherited Palaeoproterozoic lithospheric boundary between the Namibe and Epupa Zones; ii) or a tectonic boundary compensating for differential coaxial lateral forces during Mesoproterozoic times. In any case, the Serpa-Pinto strike-slip zone had a strong influence in the regional configuration of the late-Orosirian to Statherian basement (Namibe and Epupa zones) and in the following stages of the Mesoproterozoic evolution of the Angolan Shield (see section 6.4).

The origin of the ENE-WSW striking linear structure separating the Cassinga domain from the Kalahari area remains unclear. Nevertheless, the magnetic derivatives clearly reflect a high-stress concentration and suggest the existence of a large shear zone between different geological domains (Fig. 9). This structure aligns with the Opuwo Lineament in NW Namibia, which connects to the Walvis Ridge offshore Namibia (Corner et al., 2002; Fig. 1). The Opuwo Lineament is believed to have formed during Mesoproterozoic (Kibaran) to Neoproterozoic (Pan-African) times, and later reactivated during the Mesozoic as an accommodation zone during Karoo rifting (Clemson et al., 1999; Corner et al., 2002; Corner and Durrheim, 2018). A potential correlation with the Mesoproterozoic Kibaran Belt further to the northeast, beneath the Kalahari cover, is also suggested (Fig. 1). Hence, this structure may be associated with a deformational context whose time of generation must be constrained between the Mesoproterozoic HT metamorphic event recorded in the Epupa Complex of NW Namibia (ca. 1.53–1.51 Ga; Seth et al., 2003; Brandt et al., 2021) and the intrusion of the undeformed tholeiitic and alkaline-carbonatitic dikes found in NW Namibia and SW Angola (ca. 1.22–1.11 Ga; Fig. 11; Littmann et al., 2000; Kröner and Rojas-Agramonte, 2017; Salminen et al., 2018; Tshiningayamwe et al., 2022a).

Overall, the alignment of the KC magmatic rocks along NNE-SSW and E-W directions, subparallel to the Quipungo Belt and the Serpa-Pinto Line (Figs. 8-10), suggests that magma underplating and subsequent magma ascent processes occurred along large-scale pre-existing crustal weakness structures, favoured by a contractional regime. The interaction between these inherited crustal structures and the Mesoproterozoic tectono-magmatic processes was fundamental in shaping the emplacement and current architecture of the KC.

6.2. Isotopic, geochemical and structural constraints of the Kunene Complex

6.2.1. Spatio-temporal evolution and kinematic controls of long-lived magma emplacement

The U-Pb geochronological data shows that the emplacement of the anorthositic and felsic suites of the KC are the result of a long-lived magmatism throughout the Mesoproterozoic (Fig. 11). Mesoproterozoic Rb-Sr and K-Ar ages recorded in basement of SW Angola testify the thermal imprint associated with a prolonged magmatism (Fig. 10; Mendes, 1968; Silva et al., 1973; Torquato and Allsopp, 1973; Torquato and Amaral, 1973; Torquato, 1974, 1977). Similar ages are reported in the Mesoproterozoic Karagwe-Ankole and Kibarian Belts (Figs. 1B, 12; e.g., Tack et al., 2010), suggesting contemporaneous Mesoproterozoic magmatism along the southern margin of the Southwest Congo Shield.

Early Mesoproterozoic magmatism (1534 ± 3 Ma to 1498 ± 12 Ma) has been documented in the SW Angolan Shield (Fig. 2). These include poorly mapped A-type granitoids located in NW Namibia and in SW Angola (Seth et al., 1998; Luft et al., 2011; Kröner et al., 2015; Kröner and Rojas-Agramonte, 2017; Ferreira et al., 2024), as well as basic sills emplaced into the Chela Group of the Humpata Plateau (1502 ± 4 Ma; Ernst et al., 2013). The cogenetic relation between the ca. 1534–1498 Ma bimodal magmatism and the oldest KC pulses (1500 ± 1 Ma age; Bybee et al., 2019) would therefore indicate that the AMG system was magmatically active over a period of nearly 200 Ma (1534–1344 Ma; Fig. 11; Mayer et al., 2004; Seth et al., 2005; Baxe, 2007; Drüppel et al., 2007; Maier et al., 2013; McCourt et al., 2013; Bybee et al., 2019; Lehmann et al., 2020; Milani et al., 2022; this study).

The geochronological data and spatial arrangement of the KC magmatism reveal a pattern of westward rejuvenation, with older ages (1446–1424 Ma) observed in the northeastern and southeastern KC, and younger ages (1414–1344 Ma) recorded in the western segments (Fig. 10, S4). The almost consistent gravimetric response across the eastern part of the KC beneath the Kalahari basin suggests that older magmatic units are concealed in this segment (Fig. 8). Indeed, a large NNE-trending ellipsoid can be depicted when outlining the gravimetric limits in the eastern KC. Distinct NNE-trending anorthosite lobes have been recently identified in this covered eastern part (Mochales et al., 2025), segmented by highly magnetic red granites and NE-SW and NW-SE right- and left-lateral faults (Fig. 9).

Geochronological data for the central part of the western KC are still limited to two anorthosites and an undeformed megacrystic quartz-monzonite found between Pocolo and Ompupa, dated from 1414 to 1401 Ma (Fig. 2; Bybee et al., 2019; Lehmann et al., 2020). The gravimetric response and the ~ N-S trending lineaments in this area mirror those observed further south (Figs. 8, 9), suggesting that the central part of the Angolan KC predominantly consists of middle-KC igneous materials (Fig. 10). However, the presence of a mangerite dike dated at 1403 Ma (Baxe, 2007) to the west of a rhyodacite and syenogranite dated at 1446 and 1424 Ma (Figs. 2, 10) in the southeastern part of the Angolan

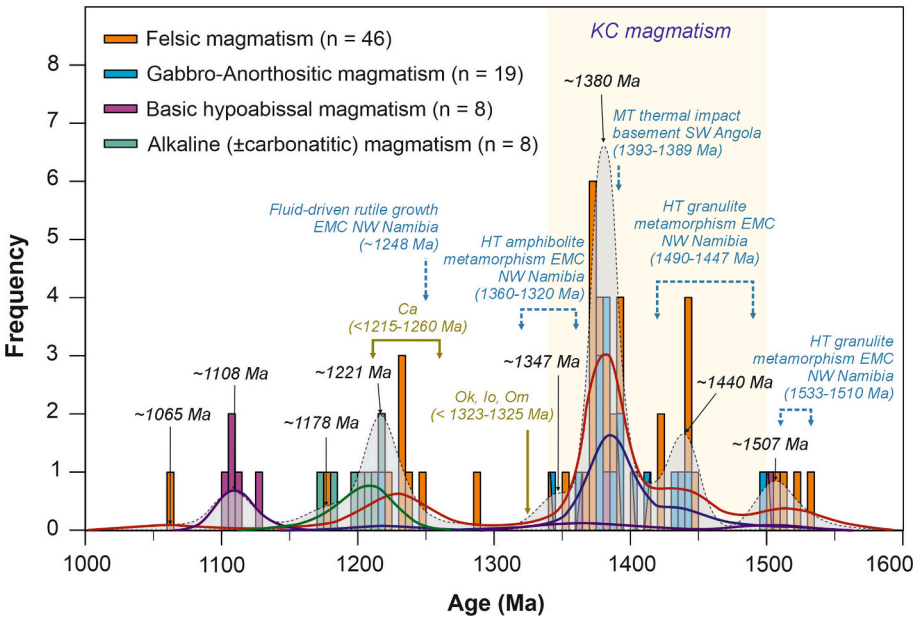

Fig. 11. Integrated Mesoproterozoic U-Pb ages recorded in SW Angola and NW Namibia, using a Kernel Density Estimation (KDE) diagram to better separate the felsic, gabbro-anorthositic, basic and alkaline-carbonatitic magmatic pulses of SW Angola and NW Namibia. The Mesoproterozoic magmatic peaks identified are constrained at ca. 1507 Ma, 1440 Ma, 1380 Ma, 1347 Ma, and between 1221–1065 Ma, these latter mainly represented in NW Namibia. The long-lasting magmatism of the Kunene Complex is highlighted in yellow (1500–1344 Ma). It is also shown the reported Mesoproterozoic U-Pb and Ar-Ar metamorphic imprints recorded in Palaeoproterozoic materials of NW Namibia and SW Angola. Maximum depositional ages for Mesoproterozoic metasedimentary sequences are also plotted for comparison (Om: Ompupa Group; Io: Iona Group; Ok: Okapuka Formation; Ca: Cahama Formation). U-Pb geochronological compilation is described in the text.

KC confirms the existence of at least three distinct pulses of felsic magmatism before 1400 Ma.

The middle- to late-KC pulses (1395–1344 Ma) are spatially confined to the highly gravimetric northwestern and southwestern segments of the KC which promoted the thermal impact from 1393 to 1389 Ma recorded in the nearby crystalline basement (Fig. 11; Lehmann et al., 2020). Highly-dipping cataclastic to mylonitic textures are displayed by both KC anorthosites and granites in these regions (Fig. S1; Bybee et al., 2019; Lehmann et al. 2020). This magmatic episode also contributed to the intrusion of some WNW-ESE trending mafic dikes west of the KC, with crystallisation ages between 1385 ± 5 Ma (Ernst et al., 2014) and 1363 ± 17 Ma (Figs. 2 and 6C). These dikes are aligned with WNW-ESE extensional fractures that transect the Palaeoproterozoic basement from the KC (Figs. 9, 10).

In the northern part of the Angolan KC, the emplacement of the 1385–1370 Ma NNE-trending mangerites and red granites of the Chiange area (collectively referred to as the Red Granite Belt; Mayer et al., 2004; McCourt et al., 2013; Lehmann et al., 2023), seems to be controlled by the NNE-trending structure that sections the gravimetric response of the older (eastern) and younger (western) KC segments (Fig. 8; Rey-Moral et al., 2022; Mochales et al., 2025). This structure resembles the remarkable positive magnetic anomaly of the region and clearly delineates a narrow, elongated, NNE-trending duplex structure (Fig. 9). In the southern part of the Angolan KC, a 1372 Ma granite dike intruding older 1442 Ma granite augen-gneiss (Fig. 2) further demonstrates the ascent of younger magmas into previously emplaced KC rocks. Indeed, anorthosites from the eastern margin of the Otchinjau lobe, dated at 1391 ± 1 Ma (Fig. 2; Bybee et al., 2019), show NNW-trending subvertical mylonitic fabrics, while the granitic facies from the western margin exhibit a steeply dipping NNE-trending mylonitic foliation (Fig. S1; Lehmann et al., 2023), resembling the structural trends depicted in the magnetic map (Fig. 9). All these features provide evidence of syn- to late-kinematic deformation during KC magmatism, likely related to the NNE-trending dextral strike-slip system suggested by the magnetic derivatives (Fig. 9).

Conversely, the E-W structural arrangement and magmatic layering of the Zebra Mountains are coherent with the Serpa Pinto strike-slip system and the Palaeoproterozoic Epupa basement (Fig. 10). P-T constraints of the upper-amphibolite facies metamorphism recorded in the Orue unit of the EC (1340–1320 Ma; Seth et al., 2005; Brandt et al., 2021), indicate significant heating at mid- to lower-crustal levels with peak conditions of 700–840 °C and 5.5–8 kbar (Brandt and Klemd, 2008), matching those estimated for anorthosites (950–985 °C and 7–9 kbar) and red granites (790–890 °C and 6.5 ± 0.6 kbar) from the Zebra lobe (Drüppel, 2003). The emplacement of slightly younger dark anorthosite pulses was likely guided by E-W trending faults, which promoted the alteration and brecciation of the white anorthosite terms. Nevertheless, the structural shifting towards N-NNE directions at the western edge of the Zebra lobe (Fig. 9) clearly indicates distortion through dextral shearing under ductile conditions (i.e., before consolidation; Drüppel, 2003).

Subsequent near-isobaric cooling to below 680 °C and ~6.2 kbar, recorded in late-stage coronitic and symplectitic assemblages in the white anorthosites, was interpreted as post-emplacement exhumation of ca. 3 km during extension (Drüppel, 2003). Nevertheless, it would also represent adiabatic ascent of material in a magma transfer zone associated with compression. Indeed, evidence of ductile shearing and brittle faulting along the contacts between the Epupa Complex (EC) and the Namibian KC (Drüppel et al., 2007; Maier et al., 2013), suggests that magma buoyancy was favoured by contractional structures, probably related to high-angle transcurrent shear zones (Fig. 9). Hence, the sheet-like configuration and the P-T trajectories estimated for the Zebra lobe would be therefore indicative of the different stages of magma ascent and subsequent configuration through thrusting and uplifting processes within a transpressive scenario, mainly controlled by the Serpa Pinto strike-slip system.

6.2.2. *Magma sources and crustal contamination*

The origin of anorthosite cumulate magmas is usually related to fractional crystallisation of upper-mantle high-Al_2O_3 tholeiitic magmas (Emslie, 1978; Silva, 1990; Ashwal, 2020), although hybridisation of mantle-derived melts with crustal components is also proposed as a

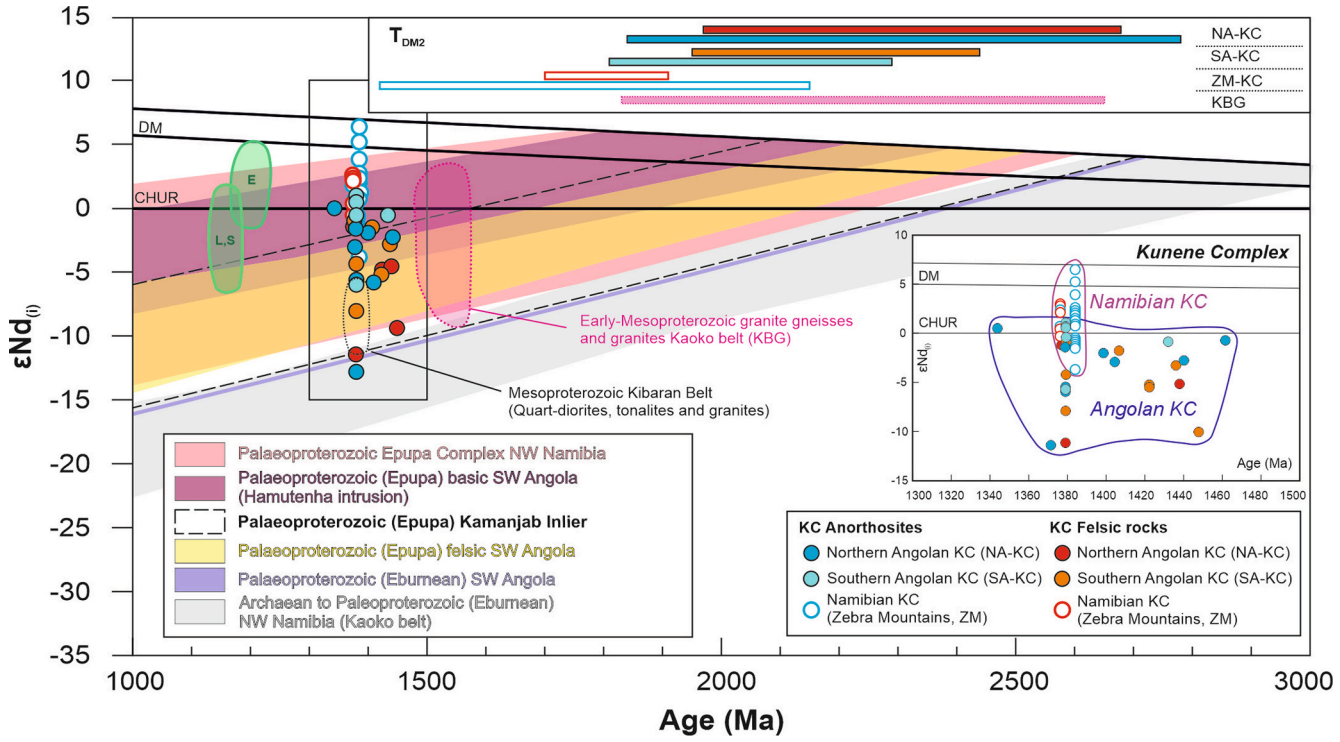

Fig. 12. Distribution of εNd values of the studied Mesoproterozoic samples, according to their crystallisation age. It is also displayed the εNd isotope composition of Early-Mesoproterozoic (1.50–1.55 Ga) granite gneisses and granite rocks cropping out within the Panafrican Kaoko Belt of NW Namibia; 1.38 Ga igneous rocks of the Kibaran Belt of the Democratic Republic of Congo; and of Late-Mesoproterozoic alkaline to carbonatitic magmas found in NW Angola and SW Angola (Lupongola, Swartbooisdrif: L,S; and Epembe: E). The εNd evolution of the distinct Archaean to Palaeoproterozoic basement of the studied area and counterparts is projected in colour-filled fields and lines: grey, Kaoko Belt of NW Namibia; violet line, SW Angola (Eburnean granite, ca. 1.95 Ga); black dashed field, Kamanjab Inlier of NW Namibia; yellow, SW Angola (Epupa felsic basement); purple, SW Angola (Epupa mafic basement); pink, Epupa Complex of NW Namibia. The calculated depleted-mantle model ages (T_{DM2}) of the KC-related Mesoproterozoic rocks from the northern Angolan-KC (NA-KC), southern Angolan-KC (SA-KC), Zebra Mountains of NW Namibia (ZM-KC) and Early-Mesoproterozoic granites and gneisses from the Kaoko Belt of NW Namibia (KBG) are shown as horizontal bars in the upper inset. The inset on the right represents an enlarged diagram exclusively displaying the ƐNd values vs age (1.30–1.50 Ga) of the Angolan and Namibian KC-anorthosites and related felsic rocks for petrological comparison. The location of the zoomed area is shown as a solid black-line box in the main diagram.

means of inferring the petrogenesis of AMCG materials (Elizondo-Pacheco et al., 2024).

The presence of orthopyroxene megacrysts, co-magmatic with anorthosite pegmatoidal enclaves (Bybee et al., 2019), indicate the anhydrous character of these magmas. Nevertheless, the high proportions of magnetite (92 %) and magnetite-hematite (48–41 %) in the gabbro-anorthosite samples (Mochales et al., 2025), and the predominant Bowen-type evolution trend followed by these materials (Fig. 3B), suggest high overall fO_2 conditions and may reflect intermediate to relatively oxidising redox conditions during the crystallisation of the parent magma (e.g., Vermeesch and Pease, 2021). The positive Sr and Eu anomalies clearly indicate plagioclase accumulation through fractional crystallisation processes, whereas the enrichment of LILE and LREE of the KC anorthosites relative to primitive mantle (PM), combined with the chondrite-normalised flat pattern of HREE, indicates a garnet-free metasomatised mantle source (Fig. 3E, G).

Nevertheless, anorthosites of the Zebra Mountains of NW Namibia and those of SW Angola exhibit notable variations in their εNd values (Fig. 12). The Namibian KC anorthosites display more radiogenic signatures, characterised by a range of εNd values spanning from −3.7 to + 6.5 (Drüppel et al., 2007, Gleißner et al., 2011). Crustal contamination mechanisms appear to be more pronounced in the external parts of the Zebra lobe (Fig. 8), consistent with higher degrees of crustal contamination near the contact with the basement. In contrast, the anorthosites of SW Angola display predominantly crustal signatures, encompassing εNd values from −12.7 to + 1.0, regardless of their crystallisation age (Fig. 12; Table 2; Slejko et al., 2002; Mayer et al., 2004; Baxe, 2007). This indicates the involvement of metasomatised enriched mantle sources or significant interaction with crustal components at source regions or during anorthosite magma ascent. The minimum Bouguer anomalies to the north and east of the KC suggest that a thicker crust underlies these areas (Fig. 8; Rey-Moral et al., 2022), which could have led to longer period of stagnation and crustal contamination of KC anorthosite magmas, presumably emplaced at middle- to upper-crustal levels (880 °C and of 3–5 kbar; Slejko et al., 2002). Overall, the geochemical and isotopic signatures of the KC gabbro-anorthosites magmas are consistent with magmas generated from an enriched mantle source with relevant crustal contribution (Figs. 3, 12), alike to those ascribed to fluctuations between mantle and crustal components within contractional contexts (e.g., Nelson and Cottle, 2018). In fact, the KC gabbro-anorthosite materials mostly plot following geochemical trends linked to convergent settings (Fig. S3; Pearce et al., 1977; Cabanis and Lecolle, 1989; Verma et al., 2006; Pearce, 2008; Hollocher et al., 2012; Saccani, 2015).

On the other hand, felsic magmas (MCG) associated with anorthosite materials are typically regarded as indicative of crustal melting or as fractionated melts derived from enriched mantle magmas (Elizondo-Pacheco et al., 2024, and references therein). The Bowen and Fenner trends characterising the subalkaline felsic samples (Fig. 3B) are indicative of the late stages of tholeiitic and calc-alkaline magma evolution (Vermeesch and Pease, 2021). Such contrasting differentiation trends may be indicative of distinct tectonic contexts; alternatively, they could be related to crustal heterogeneities, mixing of lower- and upper-crustal magmas, or crustal assimilation processes (Hora et al., 2009). The flat HREE multielement spectra of these felsic melts would be consistent with zircon melting under hot, dry conditions (i.e.- melting at < 10

kbar), as indicated by the high calculated Zr saturation temperatures (1039–799 °C; Table S1; Miller et al., 2003). The low Rb/Sr ratios of most felsic materials (< 1.0, even in samples with SiO_2 > 70 wt%) do not indicate extreme fractionation and probably reflect derivation from a primary Sr-rich and Rb-poor source (Frost and Frost, 2011). Nonetheless, no evidence of magma mingling with mantle-derived melts has been found in the KC Mesoproterozoic red granites.

The ferroan and metaluminous to peraluminous character of these felsic rocks and the geochemical patterns observed in the PM and chondrite-normalised diagrams (LILE enrichment, positive Pb and Zr anomalies, and negative Ba, Sr, Nb and Ti anomalies; Fig. 3F, H) are not compatible with magmas exclusively derived from mantle sources, suggesting a significant crustal contribution. Most geotectonic discrimination diagrams are consistent with A-type and scarce I/S-type granitoids formed by partial melting of distinct crustal protoliths during late- to post-orogenic collisional settings (Fig. S3; Batchelor and Bowden, 1985; Whalen et al., 1987; Maniar and Piccoli, 1989; Eby, 1992; Laurent et al., 2014). Indeed, partial melting of a recycled and depleted lower crust may produce felsic ferroan magmatism in distinct scenarios, including back-arc regions (Collins et al., 2019; Roberts et al., 2023). The Sr/Y and $(La/Yb)_N$ patterns shown in the KC felsic materials (Fig. S4) suggest lateral and temporal variability in cortical thickness, including crustal thinning and thickening processes, possibly related to inherited tectonic heterogeneities (Profeta et al., 2015; Lieu and Stern, 2019).

The low initial $^{87}Sr/^{86}Sr$ ratios of most red granites suggest that they were predominantly originated from anatectic melting of the lower crust (Table 2; Bassot et al., 1981; Carvalho et al., 1987; Drüppel et al., 2007, Gleißner et al., 2011). The influence of heterogeneous crustal sources (Fig. S3; Laurent et al., 2014) is also suggested by the Nd isotopic signature of these felsic materials. The red granites from SW Angola exhibit subchondritic to evolved $\varepsilon Nd_{(t)}$ values (−0.94 to −11.03, corresponding to T_{DM2} between 1.97 and 2.68 Ga; Baxe, 2007), which mostly overlap with the isotopic evolution field of the Paleoproterozoic basement of SW Angola (Fig. 12). The red granites from the Zebra Mountains display notably more radiogenic Nd isotopic signatures (from + 2.5 to −0.4; Drüppel et al., 2007), but consistent with their derivation from less evolved source materials alike to those present in the nearby Epupa Metamorphic Complex (T_{DM2} = 1.70–1.95 Ga; Fig. 12). Similar isotopically heterogeneity has also been reported in Early Mesoproterozoic (1.55–1.50 Ga) granite gneisses and granites of the Kaoko Belt of NW Namibia (Luft et al., 2011; Jung et al., 2012), as well as in the ~ 1.38 Ga quartz-diorites, tonalites and granites of the Mesoproterozoic Kibaran Belt (Debruyne et al., 2015), suggesting that isotopically heterogeneous Palaeoproterozoic protoliths were also involved in the generation of other Mesoproterozoic felsic magmatism from the Congo Craton counterparts.

6.3. *Kunene Complex sedimentary cover and regional correlations*

From the Lubango area southwards to the Oncócua region, the crystalline basement is partially covered by subhorizontal low-grade metasediments (Fig. 2). In the Humpata Plateau (Fig. 12), the low-grade metasediments that overlay the Palaeoproterozoic basement are intercalated with metavolcanic materials and covered by stromatolitic limestones at the top of the sequence (Leba Formation; Carvalho et al., 2000; Pereira et al., 2011, 2013). This sequence, known as the Chela Group, is intruded by 1.5 Ga dolerite sills at the base of the Leba formation (Fig. 2; Ernst et al., 2013). In the Oncócua Plateau (Fig. 12), the siliciclastic sequences unconformably overly the KC (Carvalho et al., 1987; Carvalho and Alves, 1990; Silva et al., 2021; Potti et al., 2021) and are intruded by Mesoproterozoic dolerites of ca. 1.13–1.10 Ga (Carvalho et al., 1987; Salminen et al., 2018), indicating a depositional age restricted between 1.34 Ga and 1.10 Ga.

The Palaeoproterozoic *meta*-volcanosedimentary Chela Group of the Humpata Plateau (1798–1750 Ma; McCourt et al., 2013) has been frequently correlated with the siliciclastic sedimentary sequences overlying the Kunene Complex (e.g., Kröner and Correia, 1980; Carvalho and Alves, 1993; Kröner and Rojas-Agramonte, 2017). However, maximum depositional ages (MDAs) of 1324 ± 10 Ma and 1184 ± 23 Ma were recently determined for the base and top of the Ompupa Group in the Oncócua Plateau, while MDAs from 1263 ± 20 to 1215 ± 13 Ma have been determined for the Cahama Formation in the Cahama region (Figs. 2, 7; Ferreira et al., 2024; this study). This would be in accordance with the presence of clasts of Mesoproterozoic red granites in the basal conglomerates of both the Ompupa Group and Cahama Formation (Carvalho et al., 1987; Escuder-Viruete and Gumiel, 2021). Moreover, a maximum depositional age of 1323 ± 13 Ma was determined for the Iona Group (Ferreira et al., 2024), thereby supporting its correlation with the contiguous Okapuka Formation of NW Namibia (1324 ± 1 Ma; Fig. 2; Kröner and Rojas-Agramonte, 2017).

The detrital zircon age intervals shown in the Cahama Formation (sample UTJEE33C008S; Fig. 7) clearly suggest: i) a contribution from Archaean materials, such are those found in the Cassinga area; ii) a large Palaeoproterozoic Eburnean-like component, similar to the granite gneisses and felsic igneous rocks described to the north and east of the KC; and iii) an equally important contribution from the Palaeoproterozoic Epupa-like basement, found to the northwest, west and south of the KC (Fig. 2). This information indicates intraplate sedimentation sourced from the surrounding pre-Mesoproterozoic basement. Nevertheless, the presence of Mesoproterozoic detrital zircons ranging from ca. 1.55 to 1.18 Ga (Fig. 7) clearly indicate exhumation, denudation, and sedimentary input from the KC and post-KC related magmatic rocks. The varying MDAs observed across metasedimentary sequences can be attributed to contrasting age components present in source rocks or the absence of Mesoproterozoic zircons reaching the basin (Ferreira et al., 2024). However, the presence of large and thick siliciclastic materials to the west of the KC (Ompupa Group on the Oncócua Plateau and Iona Group/Okapuka Formation in NW Namibia), having a higher Mesoproterozoic component (from 79 to 27 %) than that registered in the Cahama Formation (27–11 %; Ferreira et al., 2024; this study), would also suggest that the sedimentary basin becomes deeper westwards.

Similar aged intracratonic depositional activity also occur in the São Francisco craton (Espinhaço Supergroup, Brazil; e.g., Pedreira and De Waele, 2008; Guadagnin and Chemale Jr., 2015) and in the Kibaran (KiB) and Karagwe-Ankole (KAB) Belts of the Congo Craton (Kibara, Akanyaru and Kagera Supergroups; e.g., Kokonyangi et al., 2007; Fernandez-Alonso et al., 2012). These sedimentary sequences cover extensive areas (Fig. 1) and were deposited in distinct cycles from the Palaeoproterozoic (1.78–1.70 Ga) through almost the entire Mesoproterozoic (1.60 to 1.37 Ga and post-1.22 Ga). Notably, the deposition of the Ompupa Group and Cahama Formation in the SW Angola Shield occurred synchronously with the deposition of the upper sequences of the Kibara and Akanyaru Supergroups of the KiB and KAB (<1.22 Ga) and of the Upper Espinhaço sequence of the São Francisco Craton (<1.18 Ga).

Corner et al. (2002) and Corner and Durrheim (2018) interpreted the ca. 4000 to 6000 m crustal isopachs beneath Kalahari cover in southeastern Angola and northern Namibia as corresponding to Mesoproterozoic successions, bounded in the northwest and southeast by the Opuwo and Omaruru Lineaments respectively (Fig. 1B). A tentative correlation of the Opuwo Lineament with the KiB to the NE can be envisaged, suggesting that this structure may extend more than 1200 km south-westward from the known end of the KiB. This interpretation would support the continuity of the Mesoproterozoic sequences from the KAB and KiB towards SW Angola, and further west towards the São Francisco Craton (Fig. 1). Similar findings led Faleiros et al. (2024) to propose the existence of an extensive and long-lived (up to 210 Ma) early-Mesoproterozoic active margin (1570–1450 Ma) that evolved to a continental arc (1450 and 1360 Ma) at the margins of the São Francisco-Congo Cratons, followed by a continental rifting (1310–1280 Ma).

6.4. Mesoproterozoic geological evolution of the SW Angolan Shield

Even though the Mesoproterozoic basic magmatism found in Angola and Namibia has been usually related to anorogenic contexts (LIPs systems; e.g., Ernst et al., 2013, 2014; Djeutchou et al., 2023), there is still an open discussion on the petrogenesis of the Kunene Complex and related magmas, whose theories vary from intraplate (e.g., Drüppel et al., 2007; Maier et al., 2013; Pereira et al., 2013; Ernst et al., 2014) to collisional (e.g., Ashwal and Bybee, 2017; Bybee et al., 2019; Lehmann et al., 2020; Milani et al., 2022; Klausen et al., 2023) settings.

The suprachondritic eHf signatures recorded in 1.56–1.50 Ga felsic magmatism and detrital zircon components of metasedimentary sequences from SW Angola likely reflect an important juvenile input in early-Mesoproterozoic times (Ferreira et al., 2024). Conversely, a strong influence of crustal materials is reflected in 1.49 to 1.39 Ga KC materials (Fig. 12), whereas a mixed source composition dominated between 1.39 and 1.34 Ga, as evidenced by both vertical arrays of εNd and εHf signatures in KC materials and detrital zircons (Ferreira et al., 2024; this study). Such a prolonged magmatism (~200 Ma), showing this contrasting isotope evolution, would not be expected in an exclusively intracontinental anorogenic setting and may be likely linked to an evolutionary scenario involving subduction and/or lithosphere delamination processes and subsequent extension, as proposed for other Proterozoic anorthosite provinces (e.g., the Rogaland Anorthosite Province in Norway or the Musgrave orogen in Central Australia; Smithies et al., 2011, Smits et al., 2014; Slagstad et al., 2022). Indeed, the lateral and temporal distribution of Sr/Y and $(La/Yb)_N$ ratios and crystallisation temperatures of the KC felsic magmas (see Fig. S4), along with their diverse alkaline, tholeiitic and calc-alkaline affinities and evolutionary trends (Fig. 3A-B), suggests that the KC experienced an alternation between stages of thinner crust and hot magmatism, typical of an extensive or back-arc regime, and phases of lithospheric thickening, deep differentiation and crustal assimilation, associated with compressive stages (Profeta et al., 2015; Lieu and Stern, 2019).

The ENE-WSW striking linear structure connecting the Opuwo Lineament (Op-L) to the Mesoproterozoic Kibaran Belt (KiB) represents a first-order crustal boundary reflecting a transpressive environment associated with an oblique convergent margin (Figs. 1, 9). Comparable tectono-thermal and depositional activity recorded in African and Brazilian counterparts supports the potential connection through an extensive and long-lived active continental margin during the Mesoproterozoic (Faleiros et al., 2024). Lateral geochemical and isotopic heterogeneities have been described in 1.4–1.3 Ga felsic magmatism at the periphery of the Columbia Supercontinent, reflecting diachronous subduction retreat and variable crustal involvement (e.g., Wang et al., 2022). Such heterogeneities likely developed in back-arc to peripheral arc domains where subduction rollback promoted the involvement of distinct magma sources, variations in crustal thickness and assimilation processes. A similar scenario can account for the observed spatio-temporal and geochemical variability of the KC, thereby supporting a subduction-driven geodynamic setting.

Therefore, considering the protracted KC magmatism as related to a continental back-arc setting (Lehmann et al., 2020; Milani et al., 2022), mantle heat beneath the back-arc would be linked to a NNW-dipping subduction located further south of the Cassinga Zone. The alignment of early-Mesoproterozoic magmas along NNE-SSW and E-W directions, subparallel to the Quipungo Belt and Serpa Pinto Line, confirms that the magma underplating and subsequent ascent occurred along the large-scale crustal weakness structures of the pre-Mesoproterozoic basement (Fig. 13). Nevertheless, these structures are likely to be located far from the active arc and trench (Roberts et al., 2023). In addition, the consistency of deformational fabrics in both the KC materials and nearby metamorphic basement (Figs. 8-10; Fig. S1) supports the hypothesis that synkinematic magma ascent was strongly influenced by transtensional and transpressional processes under a regional contractional regime (Lehmann et al., 2020).

The estimated P-T conditions for the KC (Slejko et al., 2002; Drüppel, 2003) and the calculated temperatures for the felsic materials (up to 1039 °C; Table S1) are in agreement with the ascent of enriched mantle materials to lower crustal levels across the hot back-arc region by convective thinning, promoting the partial melting of a heterogeneous crustal sources and extensive ferroan magmatism (Fig. 3; Currie et al., 2008; Sizova et al., 2010; Roberts et al., 2023). These "anorogenic" felsic materials would likely represent the distal magmatic components of the convergent margin (Collins et al., 2019; Roberts et al., 2023). The high occurrence of granites concomitant with anorthosites would favour the diapiric sheet-like rising of the latter through deep-seated structures, due to differences in density and thermal viscosity of the granite and partially-molten wall rocks (e.g., Dobmeier, 2006). The episodic ascent of magma batches through strike-slip systems partially disrupted the structure of the previously emplaced coalescing pulses, in a westward-evolving magmatic system driven by lateral forces. The presence of Mesoproterozoic post-KC sediments overlaying the KC (<1325 Ma; Figs. 1, 13; Ferreira et al., 2024; this study), provides evidence of the rapid exhumation of the voluminous igneous materials during late Mesoproterozoic times.

Hence, our interpretation suggests a complex evolution through a series of major transtensional and transpressional systems within an overall long-lasting and extensive accretionary orogen setting from the Early to Middle Mesoproterozoic, transitioning towards an extensional regime in Late Mesoproterozoic times (Fig. 13). The integrated geochemical, isotopic, structural, and geophysical approach provides the new following insights into the Mesoproterozoic evolution of the SW Angolan Shield.

6.4.1. Early Mesoproterozoic (1540–1500 Ma)

NNW-dipping steep subduction inwards far south from the Kalahari area would produce Early Mesoproterozoic juvenile inland magmatism by mantle upwelling and decompression melting of the enriched mantle due to crustal thinning caused by back-arc extension (Fig. 13; Gianni and Luján, 2021). Large stagnation of the underplated mantle-derived magmas at the Moho could have induced ductile thinning and partial melting of the lower (to middle?) crust, leading to the emplacement of a suite of A-type granitoids (ca. 1.54–1.50 Ga; Kröner et al., 2015; Kröner and Rojas-Agramonte, 2017; Ferreira et al., 2024) and basaltic sills (ca. 1.50 Ga; Ernst et al., 2013) at shallow crustal levels along with separation and flotation of the first plagioclase-rich mushes that ascend through the crust at ca. 1.50 Ga (Bybee et al., 2019). The heat released from the ponded mantle-derived magmas likely triggered the ca. 1.53–1.51 Ga thermal metamorphism recorded in the Epembe and Eyao units of the Epupa Metamorphic Complex (970–830 °C; Fig. 11; Brandt et al., 2003, 2007; Seth et al., 2003).

6.4.2. Early to middle Mesoproterozoic transtension (1490–1420 Ma)

Progressive crustal thinning promoted near isothermal decompression (P < 6.5 kbar; Brandt et al., 2003, 2007) and medium- to high-temperature metamorphism in the Epembe unit at ca. 1.49–1.45 Ga (Pb-Pb ages in garnet; Figs. 2, 11, 13; Seth et al., 2003, 2005), which subsequently led to the emplacement of the early- to middle-KC anorthosites and red granites (1.45–1.42 Ga). The large lateral extent of the early- to middle-KC magmas (about 140 km between the presumed plutonic margins; Fig. 13) indicates significant back-arc extension in response to regional ~N-S shortening, similar to that described for other anorthosite massifs (e.g., Dobmeier, 2006). The presence of coeval subvolcanic and plutonic felsic rocks in the Cahama region (Fig. 6E-G) imply block uplift, extensive crustal thinning processes and a shallow emplacement level of these igneous bodies.

NNE-directed high-strain shearing structures in the surrounding crystalline basement, parallel to the Angolan KC arrangement, indicate that WNW-ESE extension occurred alongside with complementary strike-slip fault systems (Figs. 9, 13; Lehmann et al., 2020; this study). A juxtaposed WNW-trending dextral strike-slip system propagated

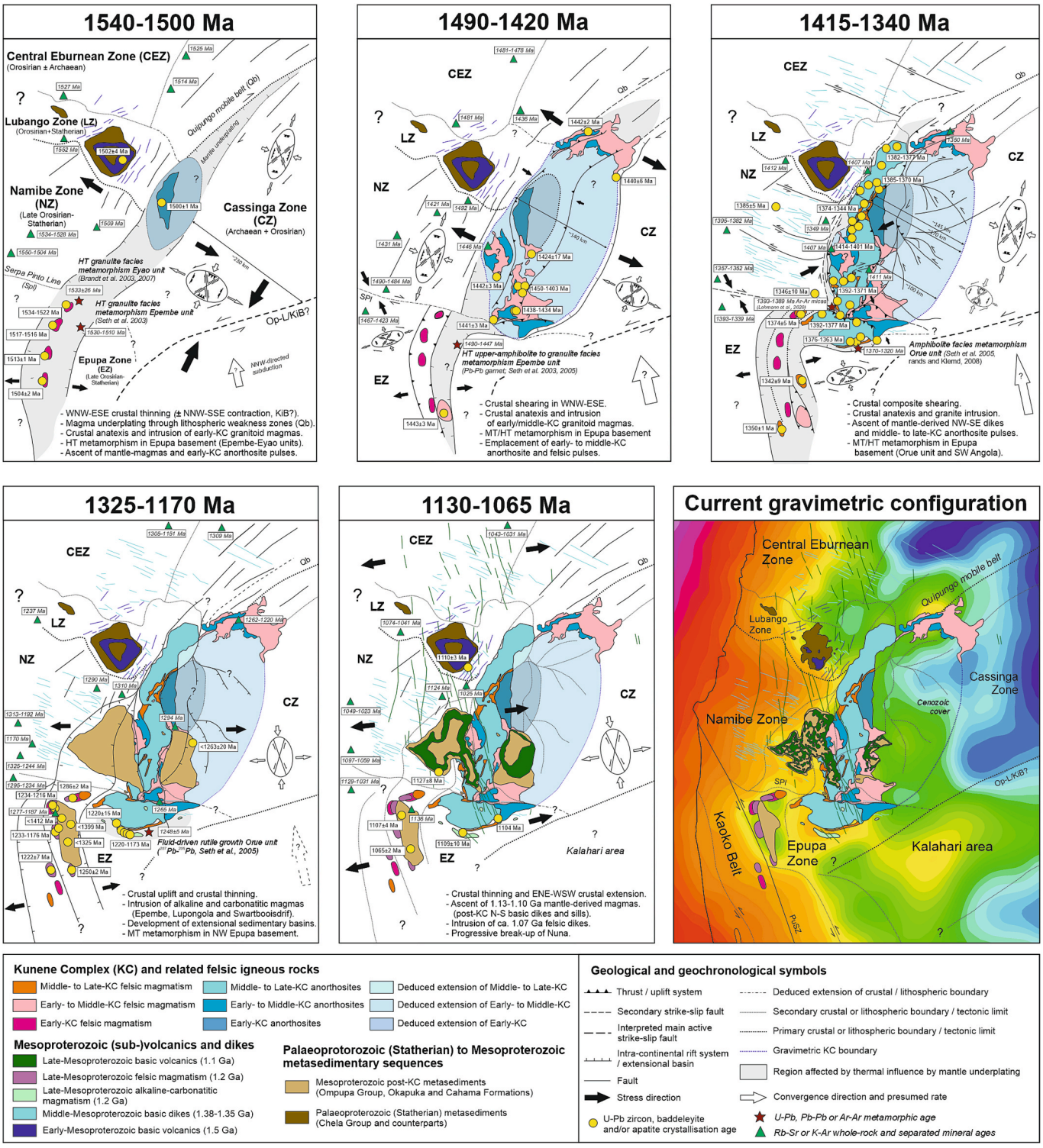

Fig. 13. Sketch diagrams showing the evolution of the Angolan Shield during the Mesoproterozoic, according to the structural, gravimetric and isotopic information discussed in this study. The diverse figures represent the main tectono-thermal magmatic and metamorphic episodes described in SW Angola and NW Namibia, responsible of the distinct ascent and emplacement of anorthosite, granite and mantle-derived melts during the distinct contractional and extensional stages. The upper figures represent the contractional scenarios in which the KC and other related magmas intruded, whereas the bottom figures display extensional post-KC stages and the current gravimetric configuration of the studied area. The distinct Palaeoproterozoic to Mesoproterozoic lithospheric boundaries and crustal structures are clearly depicted in the current gravimetric map of the studied area (modified from Rey-Moral et al., 2022), also revealing the influence of other Neoproterozoic to Cenozoic episodes occurred in the Angolan Shield, beyond the scope of this study. The U-Pb geochronological data shown in the distinct diagrams are described in the text.

through the Epupa basement and the southwestern KC margin (the Serpa-Pinto lineament; Fig. 13; Vermaak, 1981; Carvalho and Alves, 1990; Lehmann et al., 2023), separating the northern NNE-trending KC from the southern E-W trending KC. The emplacement of stagnant anorthosite magmas and related lower-crustal partial melts of the southern KC was likely favoured by antithetic thrusts from the main WNW-ESE fault, generating the elongated E-W shape and the W-trending magmatic fabrics in this southern region (Fig. 9).

6.4.3. Middle Mesoproterozoic segmented strike-slip fault system (1415–1340 Ma)

High-angle transcurrent shear zones seem to control the ascent of middle- to late-KC anorthosites and red granites. The much narrower lateral extent (Fig. 13) of the western Angolan KC pulses (about 25 km) compared to the previous ones (about 145–100 km), might indicate that transpressional processes dominated from Early to Middle Mesoproterozoic times.

The kinematic features observed in both the crystalline basement and the western Angolan KC anorthosites and red granites suggest top-to-the-west thrusting driven by E-W regional shortening and deformation synchronous with magma emplacement (Fig. 9; Lehmann et al., 2020). The "S"-shaped arrangement of middle- to late-KC pulses is indicative of transpressional shearing along a major dextral NNE-trending strike-slip system (Fig. 13). Extensional splay fractures (horsetails) developed from this main transpressive strike-slip system, promoting the intrusion of 1385–1363 Ma mantle-derived melts to the west of the KC (Figs. 9, 13; Ernst et al., 2014).

Conversely, magma ascent and configuration of the Zebra Mountains were facilitated by WNW-ESE transpressional structures, probably linked to the Serpa-Pinto dextral strike-slip system (Fig. 13). The progressive right-lateral oblique displacement under NNW-shortening stresses likely developed local restraining stepovers that overlapped northwards the Epupa basement and the middle- to late-Mesoproterozoic KC pulses, ultimately configuring the E-W trending structure found in this region.

6.4.4. Late Mesoproterozoic post-KC extensional processes (1325–1065 Ma)

Following the middle- to late-KC emplacement, the regional contractional processes ceased, with subsequent stress relaxation episodes which promoted the deposition of Late-Mesoproterozoic sediments overlaying the KC (<1325 Ma; Figs. 1, 7; Ferreira et al., 2024; this study), likely driven by the extensional reactivation of pre-existing structures through a series of block-faulting systems (Fig. 13).

Slab delamination or slab break-off processes would promote the interaction of hot asthenosphere with fertile or metasomatised lithospheric mantle, inducing the ascent of heterogeneous E-MORB to sub-lithospheric mantle melts (ca. 1220–1173 Ma Epembe, Swartbooisdrif and Lupongola alkaline to carbonatitic complexes; Figs. 2, 11–13; Littmann et al., 2000; Simon et al., 2017; Tshiningayamwe et al., 2022a,b). Additionally, decompression melting in the upper mantle and subsequent crustal anatexis promoted the emplacement of Late-Mesoproterozoic KC troctolites and A-type granitoids (1286–1176 Ma; Figs. 2, 13; Maier et al., 2013; Kröner and Rojas-Agramonte, 2017; Ferreira et al., 2024), respectively, and the medium- to high-temperature fluid activity recorded along the Angolan-Namibian frontier (1248 ± 5 Ma Pb-Pb age for rutile growth in the Orue unit and 1294–1253 Ma Rb-Sr whole-rock ages in mylonite and granite rocks; Figs. 11, 13; Torquato, 1977; Carvalho et al., 1979; Seth et al., 2005).

Further crustal extension facilitated the intrusion of the late-Mesoproterozoic ~N-S-trending basic dike and sills and minor felsic magmas (1127–1065 Ma; Figs. 10, 11, 13; Ernst et al., 2013; Kröner and Rojas-Agramonte, 2017; Salminen et al., 2018). It is presumed that progressive regional ~E-W trending crustal thinning and large-scale ~N-S directed faulting likely contributed to the final break-up of the Columbia supercontinent (Ernst et al., 2013; Salminen et al., 2018).

6.4.5. Post-Mesoproterozoic regional configuration

The current geophysical configuration of the studied area is also a consequence of the subsequent Neoproterozoic to Cenozoic deformational and tectono-thermal events that affected the SW Angolan Shield (Fig. 13). The regional effects of the E-W-trending left-lateral transpressional processes related to the Pan-African Kaoko Belt significantly restructured the pre-Neoproterozoic basement of the SW Angolan Shield (e.g., Seth et al., 1998; Goscombe et al., 2017; Konopásek et al., 2008). The fragmentation of Gondwana and the subsequent opening of the Atlantic Ocean gave rise to the pronounced gravimetric anomalies observed along the coastal margins of Angola and Namibia (Fig. 13).

7. Conclusions

The Mesoproterozoic magmatism of the southwestern Angolan Shield is indelibly marked by the Kunene Complex (KC) and related intrusions, whose emplacement occurred episodically over a protracted interval of about 200 Ma (1534–1344 Ma). Geochemical and isotopic evidence of the long-lasting KC magmatism, along with associated deformation features in both KC materials and surrounding basement, supports a potential link to a back-arc setting.

The structural arrangement and contemporaneity of deep-seated basic to anorthositic magmatism and granite melt generation suggest mantle underplating and partial melting of the lower crust along Palaeoproterozoic large-scale crustal weakness structures. The emplacement of KC magmas was structurally guided by complex NNE- and E-directed strike-slip systems that operated during the early- to middle-Mesoproterozoic. These systems likely developed in response to NNW-directed accretionary processes along an active continental margin. A potential correlation with the Kibaran Belt to the northeast, and even with the São Francisco Craton further west, is suggested, indicating a long-lived continental margin evolution characterised by oblique convergence and episodic crustal reactivation.

The late-Mesoproterozoic evolution of the southwestern Angolan Shield (i.e., <1325 Ma) is essentially characterised by a major episode of stress relaxation and extension, which promoted the exhumation of the Mesoproterozoic basement and the deposition of post-KC metasedimentary sequences. The upwelling of sub-lithospheric and other mantle-derived melts between 1234 and 1065 Ma contributed to further extensional processes that promoted the final break-up of Columbia.

CRediT authorship contribution statement

Enrique Merino-Martínez: Writing – original draft, Visualization, Supervision, Project administration, Methodology, Investigation, Formal analysis, Conceptualization. **Ezequiel Ferreira:** Writing – original draft, Visualization, Validation, Investigation, Formal analysis, Data curation, Conceptualization. **Pablo Valverde-Vaquero:** Writing – review & editing, Validation, Resources, Investigation, Funding acquisition, Formal analysis, Data curation. **José Feliciano Rodrigues:** Supervision, Project administration, Investigation. **Javier Escuder-Viruete:** Supervision, Project administration, Investigation. **José Luis García-Lobón:** Supervision, Project administration, Investigation. **Aratz Beranoaguirre:** Formal analysis, Data curation. **María del Carmen Feria:** Visualization, Investigation. **Carmen Rey-Moral:** Visualization, Investigation. **Paulo Bravo Silva:** Investigation. **Pablo González-Cuadra:** Investigation. **João Carlos Sousa:** Investigation. **Julián Potti:** Investigation. **Jaime Máximo:** Investigation. **Miguel Gutiérrez-Medina:** Investigation. **Juan Carlos Gumiel:** Investigation. **Gustavo Galán:** Investigation. **Tania Mochales:** Investigation, Funding acquisition. **José Manuel:** Supervision, Project administration, Funding acquisition. **Domingos Cordeiro:** Supervision, Project administration. **Colombo Tassinari:** Resources, Formal analysis. **Pilar Montero:** Resources, Formal analysis. **Kei Sato:** Resources, Formal analysis. **José Manuel Fuenlabrada:** Resources, Formal analysis. **Carmen Galindo:** Resources, Formal analysis.

Declaration of competing interest

The authors declare that they have no known competing financial interests or personal relationships that could have appeared to influence the work reported in this paper.

Acknowledgements

This work is a result of the National Geological Plan of Angola (PLANAGEO). This project was supported by the Government of the Republic of Angola and implemented by the Geological Survey of Angola (IGEO), under the oversight of the Angolan Ministry of Mineral Resources, Oil and Gas (MIREMPET). Analytical data and isotopic results were also supported by the subsidiary programme "Ayudas Extraordinarias Menciones Excelencia Severo Ochoa" of the CN IGME-CSIC (project AECEX2021, grant numbers 15903 and 16281). We would like to express our gratitude for the invaluable assistance provided by the local staff, who facilitated the challenging conditions during our fieldwork and geological sampling. We also highly appreciate the logistical support of Impulso Industrial Alternativo. Giselle Magdaleno Enrich (CPGeo-USP) and Virginia Sánchez López (UCM) are thanked for their assistance with the Sm-Nd isotopic analyses. The authors are also grateful for the invaluable contributions to the refinement of the article's content by Professor W.J. Collins and two anonymous reviewers, and for the commendable assistance of the Chief Editor Prof. Victoria Pease.

Appendix A. Supplementary data

Supplementary data to this article can be found online at https://doi.org/10.1016/j.precamres.2025.107937.

Data availability

All data analysed and generated during this investigation have been incorporated into the article and its supplementary information files

References

Ashwal, L.D., 1993. Anorthosites. Springer, Berlin, p. 422. https://doi.org/10.1007/978-3-642-77440-9.
Ashwal, L.D., 2020. Anorthosites. Encyclopedia of Geology, Second Edition 130–144. https://doi.org/10.1016/B978-0-12-409548-9.12461-3.
Ashwal, L.D., Bybee, G.M., 2017. Crustal evolution and the temporality of anorthosites. Earth Sci. Rev. 173, 307–330. https://doi.org/10.1016/j.earscirev.2017.09.002.
Ashwal, L.D., Twist, D., 1994. The Kunene complex, Angola/Namibia: a composite massif-type anorthosite complex. Geol. Mag. 131 (5), 579–591. https://doi.org/10.1017/S0016756800012371.
Bassot, J.P., Pascal, M., Vialette, Y., 1981. Données nouvelles sur la stratigraphie, la géochimie et la géochronologie des formations précambriennes de la partie méridionale du Haut Plateau angolais. Bulletin du Bureau de Recherches Géologiques et Minières, section 4. Géologie Générale 4, 285–309.
Batchelor, R.A., Bowden, P., 1985. Petrogenetic interpretation of granitoid rock series using multicationic parameters. Chem. Geol. 48, 43–55. https://doi.org/10.1016/0009-2541(85)90034-8.
Baxe, O.S.S., 2007. Geocronologia de Complexos máfico-ultramáficos: exemplo sa série superior do complexo de Niquelândia, Brasil e do Complexo do Kunene, Angola. Unpublished Ph.D. Thesis, Universidade de Brasilia, Instituto de Geociências, 77 p.
Boynton, W.V., 1984. Cosmochemistry of the rare earth elements: meteorite studies. In: Henderson, P., eds, Rare Earth Element Geochemistry. Elsevier, Amsterdam, pp 63-114. DOI: 10.1016/B978-0-444-42148-7.50008-3.
Brandt, S., Klemd, R., 2008. Upper-amphibolite facies partial melting of paragneisses from the Epupa complex, NW Namibia, and relations to Mesoproterozoic anorthosite magmatism. J. Metam. Geol. 26 (9), 871–893. https://doi.org/10.1111/j.1525-1314.2008.00793.x.
Brandt, S., Klemd, R., Okrusch, M., 2003. Ultrahigh-temperature metamorphism and multistage evolution of garnet-orthopyroxene granulites from the Proterozoic Epupa complex, NW Namibia. J. Petrol. 44, 1121–1144. https://doi.org/10.1093/petrology/44.6.1121.
Brandt, S., Will, T.M., Klemd, R., 2007. Magmatic loading in the proterozoic Epupa complex, NW Namibia, as evidenced by ultrahigh-temperature sapphirine-bearing orthopyroxene–sillimanite–quartz granulites. Precambr. Res. 153, 143–178. https://doi.org/10.1016/j.precamres.2006.11.016.
Brandt, S., Klemd, R., Xie, H., Bobek, P., 2021. Unravelling the P-T-t history of three high-grade metamorphic events in the Epupa complex, NW Namibia: Implications for the Paleoproterozoic to Mesoproterozoic evolution of the Congo Craton. Am. J. Sci. 321 (1–2), 235–296. https://doi.org/10.2475/01.2021.07.
Brower, A.M., 2017. Understanding Magmatic Timescales and Magma Dynamics in Proterozoic Anorthosites: a Geochronological and Remote Sensing Investigation of the Kunene Complex, Angola. Unpublished PhD Dissertation, University of Witwatersrand, Johannesburg, South Africa, 86 p.
Buzzi, J., Gutiérrez-Medina, M., 2022. Carta Geológica de Angola à escala 1:250.000, Folha Sul D-33/X, Cassinga, e Notícia Explicativa. Ministério dos Recursos Minerais, Petróleo e Gás, UTE PLANAGEO (IGME-LNEG-Impulso) - Instituto Geológico de Angola (IGEO), Luanda, Angola, 140 p.
Bybee, G.M., Hayes, B., Owen-Smith, T.M., Lehmann, J., Ashwal, L.D., Brower, A.M., Hill, C.M., Corfu, F., Manga, M., 2019. Proterozoic massif-type anorthosites as the archetypes of long-lived (≥100 Myr) magmatic systems—New evidence from the Kunene Anorthosite complex, Angola. Precambrian Research 332, 105393. https://doi.org/10.1016/j.precamres.2019.105393.
Cabanis, B., Lecolle, M., 1989. Le diagramme La/10-Y/15-Nb/8: un outil pour la discrimination des séries volcaniques et la mise en évidence des processus de mélange et/ou de contamination crustale. Comptes Rendus De L'académie Des Sciences - Series IIA 309, 2023–2029.
Campeny, M., Proenza, J.A., Castillo-Oliver, M., Torró, L., Villanova-de-Benavent, C., Melgarejo, J.C., Gonçalves, A.O., Román-Alpiste, M.J., Blanco-Quintero, I.F., Llovet, X., Farré-de-Pablo, J., 2023. Petrology, metallogeny and U-Pb geochronology of the Paleoproterozoic mafic-ultramafic Hamutenha intrusion, Angolan Shield. J. Afr. Earth Sc. 197, 104733. https://doi.org/10.1016/j.jafrearsci.2022.104733.
Carvalho, H., 1982. Geologia de Angola, Geological map of Angola. Instituto Investigação Científica Tropical, Centro Geologia, Lisboa, 4 sheets, escale 1: 1.000.000.
Carvalho, H., 1984. Estratigrafia do Précâmbrico de Angola. Garcia De Orta, Serie Geologia, Lnstituto Investigação Científica Tropical 7 (1–2), 1–66.
Carvalho, H., Alves, P., 1990. Gabbro-Anorthosite Complex of SW Angola/NW Namibia. Comunicações Instituto de Investigação Científica Tropical, Portugal, Série de Ciências da Terra, 2, Lisboa, pp. 5–64.
Carvalho, H., Alves, P., 1993. The Precambrian of SW Angola and NW Namibia: General Remarks, Correlation Analysis, Economic Geology. Comunicações Instituto de Investigação Científica Tropical, Portugal, Série de Ciências da Terra, 4, Lisboa, 38 p.
Carvalho, H., Tassinari, C., 1992. Idades do magmatismo granítico da região de Caraculo-Bibala, SW de Angola e suas implicações na correlação geológica com o cinturão Ribeira no sudeste do Brasil. Revista Brasileira De Geociências 22 (1), 73–81.
Carvalho, H., Fernandez, A., Vialette, Y., 1979. Chronologie absolue du Précambrien du Sud-Ouest de L'Angola. Comptes Rendus De L'académie Des Sciences Paris 288, 1647–1650.
Carvalho, H., Crasto, J.P., Silva, Z.C.G., Vialette, Y., 1987. The Kibaran cycle in Angola — a discussion. Geol. J. 22, 85–102. https://doi.org/10.1002/gj.3350220609.
Carvalho, H., Tassinari, C.C., Alves, P.H., Guimarães, F., Simões, M., 2000. Geochronological review of the Precambrian in western Angola: links with Brazil. J. Afr. Earth Sc. 31 (2), 383–402. https://doi.org/10.1016/S0899-5362(00)00095-6.
Chemale, F., Philipp, R.P., Dussin, I.A., Liquintinie Formoso, M.L., Kawashita, K., Berttotti, A.L., 2011. Lu–Hf and U–Pb age determination of Capivarita Anorthosite in the Dom Feliciano Belt, Brazil. Precambrian Research 186 (1–4), 117–126. https://doi.org/10.1016/j.precamres.2011.01.005.
Clemson, J., Cartwright, J., Swart, R., 1999. The Namib Rift: a rift system of possible Karoo age, offshore Namibia. In. Cameron, N.R., Bate, R.H. Clure, V.S. (eds), The Oil and Gas Habitats of the South Atlantic. Geological Society of London, Special Publications 153, 381-402. DOI: 10.1144/GSL.SP.1999.153.01.23.
Collins, W.J., Huang, H.-Q., Bowden, P., Kemp, A.I.S., 2019. Repeated S–I–A-type granite trilogy in the Lachlan Orogen and geochemical contrasts with A-type granites in Nigeria: implications for petrogenesis and tectonic discrimination. Geological Society of London, Special Publications 491. https://doi.org/10.1144/SP491-2018-159.
Condie, K.C., Pisarevsky, S.A., Puetz, S.J., Roberts, N.M.W., Spencer, C.J., 2023. A-type granites in space and time: Relationship to the supercontinent cycle and mantle events. Earth Planet. Sci. Lett. 610, 118125. https://doi.org/10.1016/j.epsl.2023.118125.
Corner, B., Durrheim, R.J., 2018. An Integrated Geophysical and Geological Interpretation of the Southern African Lithosphere. In: S. Siegesmund et al. (eds.), Geology of Southwest Gondwana, Regional Geology Reviews. DOI: 10.1007/978-3-319-68920-3_2.
Corner, B., Cartwright, J., Swart, R., 2002. Volcanic passive margin of Namibia: a potential fields perspective. Geol. Soc. Am. Spec. Pap. 362, 203–220. https://doi.org/10.1130/0-8137-2362-0.203.
Currie, C.A., Huismans, R.S., Beaumont, C., 2008. Thinning of continental backarc lithosphere by flow-induced gravitational instability. Earth Planet. Sci. Lett. 269 (3), 436–447. https://doi.org/10.1016/j.epsl.2008.02.037.
Debon, F., Le Fort, P., 1983. A chemical-mineralogical classification of common plutonic rocks and associations. Trans. R. Soc. Edinb. Earth Sci. 73, 135–149.
Debon, F., Le Fort, P., 1988. A cationic classification of common plutonic rocks and their magmatic associations: principles, method, applications. Bulletin of Mineralogy 111, 493–511.
Debruyne, D., Hulsbosch, N., Van Wilderode, J., Balcaen, L., Vanhaecke, F., Muchez, P., 2015. Regional geodynamic context for the Mesoproterozoic Kibara Belt, KIB and the Karagwe-Ankole Belt: evidence from geochemistry and isotopes in the KIB. Precambr. Res. 264, 82–97. https://doi.org/10.1016/j.precamres.2015.04.001.

Delhal, J., Ledent, D., Cordani, U.G., 1969. Ages Pb/U, Sr/Rb et Ar/K de Formations Métamorphiques et Granitiques du Sud-Est du Brésil, états de Rio de Janeiro et Minas Gerais. Annales De La Société Géologique De Belgique 92, 271–283.

Delhal, J., Ledent, D., Torquato, J.R., 1976. Nouvelles données géochronologiques relatives au complexe gabbro-noritique et charnockitique du bouclier du Kasai et à son prolongement en Angola. Annales De La Société Géologique De Belgique 99, 211–226. https://popups.uliege.be/0037-9395/index.php?id=5361.

Delor, C., Lafon, J. M., Rossi, P., Cage, M., Pato, D., Chevrel, S. Lê Metour, J., Matukov, D., Sergeev, S., 2006. Unravelling Precambrian crustal growth of central west Angola: Neoarchaean to Siderian inheritance, main Orosirian accretion and discovery of the "Angolan" Pan African Belt. In: Abstract of the 21st Colloquium of African Geology, Maputo, Mozambique, pp. 3-5.

De Waele, B., Johnson, S.P., Pisarevsky, S.A., 2008. Palaeoproterozoic to Neoproterozoic growth and evolution of the eastern Congo Craton: its role in the Rodinia puzzle. Precambr. Res. 160, 127–141. https://doi.org/10.1016/j.precamres.2007.04.020.

De Wit, M.J., Linol, B., 2015. Precambrian Basement of the Congo Basin and its flanking terrains. In: de Wit, M.J. (ed.), Geology and Resource Potential of the Congo Basin, Regional Geology Reviews. Springer-Verlag Berlin Heidelberg. 417 p. DOI: 10.1007/978-3-642-29482-2_2.

Djeutchou, C., de Kock, M., Ernst, R.E., Ossa Ossa, F., Bekker, A., 2023. A review of the Intraplate Mafic Magmatic Record of the Greater Congo craton. Earth Sci. Rev. 249, 104649. https://doi.org/10.1016/j.earscirev.2023.104649.

Dobmeier, C., 2006. Emplacement of Proterozoic massif-type anorthosite during regional shortening: evidence from the Bolangir anorthosite complex, Eastern Ghats Province, India. Int. J. Earth Sciences, Geologische Rundschau 95, 543–555. https://doi.org/10.1007/s00531-005-0050-x.

Drüppel, K., 2003. Petrogenesis of the Mesoproterozoic anorthosite, syenite and carbonatite suites of NW Namibia and their contribution to the metasomatic formation of the Swartbooisdrif sodalite deposits. PhD Rer. Nat. thesis, University of Würzburg. 345 p.

Drüppel, K., Brandt, S., Okrusch, M., 2000. Evolution of the anorthositic Kunene intrusive complex and the metamorphic rocks of the Epupa complex, NW Namibia: Evidence for cogenetic formation during Proterozoic crustal extension? GeoLuanda 2000, International Conference, Abstract Volume, 47–48.

Drüppel, K., Littmann, S., Romer, R.L., Okrusch, M., 2007. Petrology and isotopic geochemistry of the Mesoproterozoic anorthosite and related rocks of the Kunene Intrusive complex, NW Namibia. Precambr. Res. 156, 1–31. https://doi.org/10.1016/j.precamres.2007.02.005.

Duchesne, J.C., Maquil, R., Demaiffe, D., 1985. The Rogaland Anorthosites: Facts and Speculations. In: Tobi, A.C., Touret, J.L.R. (eds) The Deep Proterozoic Crust in the North Atlantic Provinces. NATO ASI Series, vol 158. Springer, Dordrecht. DOI: 10.1007/978-94-009-5450-2_27.

Eby, N., 1992. Chemical subdivision of the A-type granitoids: Petrogenetic and tectonic implications. Geology 20, 641–644.

Elizondo-Pacheco, L.A., Solari, L.A., González-Guzmán, R., He, H.L., Becerra-Torre, E., Ramírez-Fernández, J.A., Maldonado, R., 2024. Multi-isotope and geochemical approach to the magma source and tectonic setting of Proterozoic anorthosite massifs and Anorthosite-Mangerite-Charnockite-Granite, AMCG Suites. Geoscience Frontiers 15 (6), 101880. https://doi.org/10.1016/j.gsf.2024.101880.

Emslie, R.F., 1978. Anorthosite massifs, rapakivi granites, and late proterozoic rifting of north America. Precambr. Res. 7 (1), 61–98. https://doi.org/10.1016/0301-9268(78)90005-0.

Emslie, R.F., Hamilton, M.A., Thériault, R.J., 1994. Petrogenesis of a Mid-Proterozoic Anorthosite-Mangerite-Charnockite- Granite (AMCG) Complex: Isotopic and Chemical Evidence from the Nain Plutonic Suite. J. Geol. 102, 539–558. https://doi.org/10.1086/629697.

Ernst, R.E., Pereira, E., Hamilton, M.A., Van-Dunem, M.V., Rodriques, J., Tassinari, C.C., Teixeira, W., 2013. Mesoproterozoic intraplate magmatic 'barcode' record of the Angola portion of the Congo Craton: newly dated magmatic events at 1505 and 1110 Ma and implications for Nuna (Columbia) supercontinent reconstructions. Precambr. Res. 230, 103–118. https://doi.org/10.1016/j.precamres.2013.01.010.

Ernst, R.E., Söderlund, U., Fieldhouse, I., 2014. 1385±5 Ma U-Pb age for the WNW-trending Virei dyke swarm of SW Congo craton: part of the plumbing system for the Kunene Complex, and implications for the broader ca. 1385-1375 Ma LIP on multiple blocks. Unpublished LIPs-Industry Consortium Report A157, 1 – 7. In: Reconstruction of Supercontinents Back To 2.7 Ga Using The Large Igneous Province, LIP Record: With Implications For Mineral Deposit Targeting, Hydrocarbon Resource Exploration, and Earth System Evolution. www.supercontinent.org.

Escuder-Viruete, J., Gumiel, J.C., 2021. Carta Geológica de Angola à escala 1:250.000, Folhas Sul E-33/C e Sul E-33/I, Cahama, e Notícia Explicativa. Ministério dos Recursos Minerais, Petróleo e Gás, UTE PLANAGEO (IGME-LNEG-Impulso) - Instituto Geológico de Angola (IGEO), Luanda, Angola, 249 p.

Escuder-Viruete, J., Gumiel, J.C., Merino, E., Da Cruz Correia, J., Quintana, L., 2021. Carta Geológica de Angola à escala 1:250.000, Folhas Sul D-33/S e Sul D-32/Z, Namibe, e Notícia Explicativa. Ministério dos Recursos Minerais, Petróleo e Gás, UTE PLANAGEO (IGME-LNEG-Impulso) - Instituto Geológico de Angola (IGEO), Luanda, Angola, 188 p.

Evans, D.A.D., Mitchell, R.N., 2011. Assembly and breakup of the core of Paleoproterozoic-Mesoproterozoic supercontinent Nuna. Geology 39, 443–446.

Faleiros, F.M., Ribeiro, B.V., Forero-Ortega, A.J., Campanha, G.A.C., Cawood, P.A., 2024. Decoding Calymmian juvenile mafic magmatism in the Ribeira Belt, Brazil: evidence for a long-lived arc system along the margin of Columbia. Precambr. Res. 414, 107588. https://doi.org/10.1016/j.precamres.2024.107588.

Fernandez-Alonso, M., Cutten, H., De Waele, B., Tack, L., Tahona, A., Baudet, D., Barritt, S.D., 2012. The Mesoproterozoic Karagwe-Ankole Belt, formerly the NE Kibara Belt: the result of prolonged extensional intracratonic basin development punctuated by two short-lived far-field compressional events. Precambr. Res. 216–219, 63–86.

Ferreira, E., Lehmann, J., Rodrigues, J.F., Hayes, B., Merino-Martinez, E., Milani, l., Owen- Smith, T.M., Bybee, G.M., Tassinari, C., Ueckermann, H., Silva, P.B., Correia, J., Labaredas, J., Duarte, L., Molekwa, A.M., Sato, K., Manuel, J., da Mata, A., Victorino, L., 2024. Zircon U-Pb and Lu-Hf isotopes reveal the crustal evolution of the SW Angolan Shield, Congo Craton. Gondwana Research 131, 317-342. DOI: 10.1016/j.gr.2024.03.010.

Frost, C.D., Frost, B.R., 2011. On ferroan (A-type) granitoids: their compositional variability and modes of origin. J. Petrol. 52, 39–53. https://doi.org/10.1093/petrology/egq070.

Galán, G., 2021. Carta Geológica de Angola à escala 1:250.000, Folha Sul D-33/O, Quipungo, e Notícia Explicativa. Ministério dos Recursos Minerais, Petróleo e Gás, UTE PLANAGEO (IGME-LNEG-Impulso) - Instituto Geológico de Angola (IGEO), Luanda, Angola, 194 p.

Gianni, G.M., Luján, S.P., 2021. Geodynamic controls on magmatic arc migration and quiescence. Earth Sci. Rev. 218, 103676. https://doi.org/10.1016/j.earscirev.2021.103676.

Gleißner, P., Drüppel, K., Romer, R.L., 2011. The role of crustal contamination in massif-type anorthosites, new evidence from Sr–Nd–Pb isotopic composition of the Kunene Intrusive complex, NW Namibia. Precambr. Res. 185, 18–36. https://doi.org/10.1016/j.precamres.2010.11.004.

Gonçalves, A.O., 2010. Caracterización mineralógica, geoquímica y petrogenética de las pegmatitas graníticas de Giraúl, Namibe Angola. Unpublished Ph.D. Thesis, University of Zaragoza, Spain. 764 p.

Goscombe, B., Foster, D.A., Gray, D., Wade, B., Marsellos, A., Titus, J., 2017. Deformation correlations, stress field switches and evolution of an orogenic intersection: the Pan-African Kaoko-Damara orogenic junction, Namibia. Geosci. Front. 8, 1187–1232. https://doi.org/10.1016/j.gsf.2017.05.001.

Guadagnin, F., Chemale, F., 2015. Detrital zircon record of the Paleoproterozoic to Mesoproterozoic cratonic basins in the São Francisco Craton. J. S. Am. Earth Sci. 60, 104–116. https://doi.org/10.1016/j.jsames.2015.02.007.

Gutiérrez-Medina, M., 2022. Carta Geológica de Angola à escala 1:250.000, Folha Sul D-33/M, Munhino, e Notícia Explicativa. Ministério dos Recursos Minerais, Petróleo e Gás, UTE PLANAGEO (IGME-LNEG-Impulso) - Instituto Geológico de Angola (IGEO), Luanda, Angola, 236 p.

Hanson, R.E., 2003. Proterozoic geochronology and tectonic evolution of southern Africa. SP 206, 427–463. https://doi.org/10.1144/GSL.SP.2003.206.01.20.

Hollocher, K., Robinson, P., Walsh, E., Roberts, D., 2012. Geochemistry of amphibolite-facies volcanics and gabbros of the Storen Nappe in extensions west and southwest of Trondheim, western gneiss region, Norway: a key to correlations and paleotectonic settings. American Journal of Sciences 312, 357–416. https://doi.org/10.2475/04.2012.01.

Hora, J.M., Singer, B.S., Wörner, G., Beard, B.L., Jicha, B.R., Johnson, C.M., 2009. Shallow and deep crustal control on differentiation of calc-alkaline and tholeiitic magma. Earth Planet. Sci. Lett. 285, 75–86. https://doi.org/10.1016/j.epsl.2009.05.042.

Irvine, T.M., Baragar, W.R., 1971. A guide to the chemical classification of common volcanic rocks. Can. J. Earth Sci. 8, 523–548. https://doi.org/10.1139/e71-055.

Jelsma, H., Perritt, S-H., Armstrong. R.A, Ferreira, H.F., 2011. SHRIMP U–Pb zircon geochronology of basement Rocks of the Angolan Shield, western Angola. In: Proceedings of the 23rd CAG, Johannesburg. Council for Geoscience, Pretoria, 203 (3), 395-409.

Jelsma, H.A., McCourt, S., Perritt, S.H., Armstrong, R.A., 2018. The Geology and Evolution of the Angolan Shield, Congo Craton, in: Siegesmund, S., Basei, M.A.S., Oyhantçabal, P., Oriolo, S. (eds.), Geology of Southwest Gondwana, Regional Geology Reviews. Springer International Publishing, Cham, pp. 217–239. DOI: 10.1007/978-3-319-68920-3_9.

Jung, S., Mezger, K., Nebel, O., Kooijman, E., Berndt, J., Hauff, F., Münker, C., 2012. Origin of Meso-Proterozoic post-collisional leucogranite suites, Kaokoveld, Namibia: constraints from geochronology and Nd, Sr, Hf, and Pb isotopes. Contrib. Miner. Petrol. 163, 1–17. https://doi.org/10.1007/s00410-011-0655-y.

Klausen, M., Geldenhuys, P., Evans, D., Söderlund, U., Ernst, R., Hanson, R., Salminen, J., Trindade, R., Fieldhouse, I., 2023. Potential Kunene-related mafic dyke swarms. Geocrongress 2023 Conference Abstract, Stellenbosch, South Africa. https://allevents.eventsair.com/geocongress/.

Kokonyangi, J.W., Kampunzu, A.B., Armstrong, R., Arima, M., Yoshida, M., Okudaira, T., 2007. U-Pb SHRIMP Dating of Detrital Zircons from the Nzilo Group, Kibaran Belt: Implications for the source of Sediments and Mesoproterozoic Evolution of Central Africa. J. Geol. 115, 99–113. https://doi.org/10.1086/509270.

Konopásek, J., Košler, J., Tajčmanová, L., Ulrich, S., Kitt, S.L., 2008. Neoproterozoic igneous complex emplaced along major tectonic boundary in the Kaoko Belt, NW Namibia: ion probe and LA-ICP-MS dating of magmatic and metamorphic zircons. J. Geol. Soc. London 165 (1), 153–165. https://doi.org/10.1144/0016-76492006-192.

Korpershoek, H., 1970. Geology of the Cassinga north area; explanatory note of the 1/50,000 geological map. Companhia Mineira do Lobito, unpublished report.

Korpershoek, H.R., 1984. The geology of the Cassinga district, Angola and its potential as compared to that of the Serra dos Carajás, Brazil. 33 Congresso Braisileiro Geologia, Rio de Janeiro, Brasil.

Kröner, A., Correia, H., 1980. Continuation of the Pan African Damara Belt into Angola: a proposed correlation of the Chela Group in Southern Angola with the Nosib Group in Northern Namibia/SWA. South Africa J. Geol. 83, 5–16.

Kröner, A., Rojas-Agramonte, Y., 2017. Mesoproterozoic, Grenville-age granitoids and supracrustal rocks in Kaokoland, northwestern Namibia. Precambr. Res. 298, 572–592. https://doi.org/10.1016/j.precamres.2017.07.008.
Kröner, S., Konopásek, J., Kröner, A., Passchier, C.W., Poller, U., Wingate, M.T.D., Hofmann, K.-H., 2004. U-Pb and Pb-Pb zircon ages for metamorphic rocks in the Kaoko Belt of Northwestern Namibia: A Palaeo- to Mesoproterozoic basement reworked during the Pan-African orogeny. S. Afr.J. Geol. 107, 455–476. https://doi.org/10.2113/107.3.455.
Kröner, A., Rojas-Agramonte, Y., Hegner, E., Hoffmann, K.-H., Wingate, M.T.D., 2010. SHRIMP zircon dating and Nd isotopic systematics of Palaeoproterozoic migmatitic orthogneisses in the Epupa Metamorphic complex of northwestern Namibia. Precambr. Res. 183, 50–69. https://doi.org/10.1016/j.precamres.2010.06.018.
Kröner, A., Rojas-Agramonte, Y., Wong, J., Wilde, S.A., 2015. Zircon reconnaissance dating of Proterozoic gneisses along the Kunene River of northwestern Namibia. Tectonophysics 662, 125–139. https://doi.org/10.1016/j.tecto.2015.04.020.
Labaredas, J., Correia, J., Rodrigues, J. F., 2021. Carta Geológica de Angola à escala 1: 250.000, Folhas Sul E-33/A, Espinheira, e Notícia Explicativa. Ministério dos Recursos Minerais, Petróleo e Gás, UTE PLANAGEO (IGME-LNEG-Impulso) - Instituto Geológico de Angola (IGEO), Luanda, Angola, 158 p.
Langa, W.M., 2019. The petrology and economic potential of mafic- ultramafic intrusions west of the Kunene Anorthosite Complex, SW Angola. Unpusblished Ph.D. Thesis, University of Johannesburg. 114 p.
Laurent, O., Martin, H., Moyen, J.F., Doucelance, R., 2014. The diversity and evolution of late-Archean granitoids: evidence for the onset of 'modern-style' plate tectonics between 3.0 and 2.5 Ga. Lithos 205, 208–235. https://doi.org/10.1016/j.lithos.2014.06.012.
Lehmann, J., Bybee, G.M., Hayes, B., Owen-Smith, T.M., Belyanin, G., 2020. Emplacement of the giant Kunene AMCG complex into a contractional ductile shear zone and implications for the Mesoproterozoic tectonic evolution of SW Angola. Int. J. Earth Sci. 109, 1463–1485. https://doi.org/10.1007/s00531-020-01837-5.
Lehmann, J., Brower, A.M., Owen-Smith, T.M., Bybee, G.M., Hayes, B., 2023. Landsat 8 and Alos DEM geological mapping reveals the architecture of the giant Mesoproterozoic Kunene complex anorthosite suite (Angola/Namibia). Geosci. Front. 14, 101620. https://doi.org/10.1016/j.gsf.2023.101620.
Lieu, W.K., Stern, R.J., 2019. The robustness of Sr/Y and La/Yb as proxies for crust thickness in modern arcs. Geosphere 15 (3), 621–641. https://doi.org/10.1130/GES01667.1.
Littmann, S., Romer, R.L., Okrusch, M., 2000. Nephelinsyenite der Epembe-Swartbooisdrif-Alkali-Provinz (ESAP)/NW Namibia. Berichte Der Deutschen Mineralogischen Gesellschaft, Beihefte Zum European Journal of Mineralogie 12, 115.
Ludwig, K.R., 2012. User's manual for Isoplot 3.75, a geochronological toolkit for Microsoft Excel. Berkeley Geochronology Center Special Publication No. 5.
Luft, J.L., Chemale, F., Armstrong, R., 2011. Evidence of 1.7- to 1.8-Ga Collisional Arc in the Kaoko Belt, NW Namibia. Int.J. Earth Sci., Geol Rundsch. 100, 305–321. https://doi.org/10.1007/s00531-010-0591-5.
Machado, N., Valladares, C., Heilbron, M., Valeriano, C., 1996. U-Pb geochronology of the central Ribeira belt, Brazil and implications for the evolution of the Brazilian orogeny. Precambrian Res. 79 (3–4), 347–361. https://doi.org/10.1016/0301-9268(95)00103-4.
Maier, W.D., Rasmussen, B., Fletcher, I.R., Li, C., Barnes, S.-J., Huhma, H., 2013. The Kunene Anorthosite complex, Namibia, and its Satellite Intrusions: Geochemistry, Geochronology, and Economic potential. Econ. Geol. 108, 953–986. https://doi.org/10.2113/econgeo.108.5.953.
Maniar, P.D., Piccoli, P.M., 1989. Tectonic discrimination of granitoids. Geol. Soc. Am. Bull. 101, 635–643. https://doi.org/10.1130/0016-7606(1989)101<0635:TDOG>2.3.CO;2.
Marimon, R.S., Johannes Trouw, R.A., Dantas, E.L., Ribeiro, A., 2020. U-Pb and Lu-Hf isotope systematics on detrital zircon from the southern São Francisco Craton's Neoproterozoic passive margin: Tectonic implications. J. S. Am. Earth Sci. 100, 102539. https://doi.org/10.1016/j.jsames.2020.102539.
Mayer, A., Hofmann, A.W., Sinigoi, S., Morais, E., 2004. Mesoproterozoic Sm–Nd and U–Pb ages for the Kunene Anorthosite complex of SW Angola. Precambr. Res. 133, 187–206. https://doi.org/10.1016/j.precamres.2004.04.003.
McCourt, S., Armstrong, R.A., Jelsma, H., Mapeo, R.B.M., 2013. New U–Pb SHRIMP ages from the Lubango region, SW Angola: insights into the Palaeoproterozoic evolution of the Angolan Shield, southern Congo Craton, Africa. JGS 170, 353–363. https://doi.org/10.1144/jgs2012-059.
McDonough, W., Sun, S.S., 1995. The composition of the Earth. Chem. Geol. 120, 223–253. https://doi.org/10.1016/0009-2541(94)00140-4.
Meert, J.G., 2012. What's in a name? the Columbia, Paleopangaea/Nuna supercontinent. Gondw. Res. 21, 987–993. https://doi.org/10.1016/j.gr.2011.12.002.
Meert, J.G., Santosh, M., 2017. The Columbia supercontinent revisited. Gondw. Res. 50, 67–83.
Mendes, F., 1968. Mesures Géochronologiques en Angola. PhD Thesis, Clermont-Ferraud University, Clermont, France, 21 p.
Merino-Martínez, E., 2022. Carta Geológica de Angola à escala 1:100.000, Folha 336, Lubango, e Notícia Explicativa. Ministério dos Recursos Minerais, Petróleo e Gás, UTE PLANAGEO (IGME-LNEG-Impulso) - Instituto Geológico de Angola (IGEO), Luanda, Angola, 171 p.
Merino-Martínez, E., Goicoechea, P.P., 2022. Carta Geológica de Angola à escala 1: 250.000, Folha SUL D-33/N, Lubango, e Notícia Explicativa. Ministério dos Recursos Minerais, Petróleo e Gás, UTE PLANAGEO (IGME-LNEG-Impulso) - Instituto Geológico de Angola (IGEO), Luanda, Angola, 244 p.
Merino-Martínez, E., Rodrigues, J.F., Ferreira, E., Chamizo, M., Potti, J., Labaredas, J., Francés, A., Morais, A. Oliveira, A., Pereira, E., 2022. Mapa Geológico de Angola à escala 1:1.000.000, e Notícia Explicativa. Zona UTE, Região Sul de Angola. Ministério dos Recursos Minerais, Petróleo e Gás, UTE PLANAGEO (IGME-LNEG-Impulso) - Instituto Geológico de Angola (IGEO), Luanda, Angola, 105 p.
Middlemost, E.A.K., 1994. Naming materials in the magma/igneous rock system. Earth Sci. Rev. 37, 215–224. https://doi.org/10.1016/0012-8252(94)90029-9.
Milani, L., Lehmann, J., Bybee, G.M., Hayes, B., Owen-Smith, T.M., Oosthuizen, L., Delport, P.W.J., Ueckermann, H., 2022. Geochemical and geochronological constraints on the Mesoproterozoic Red Granite Suite, Kunene AMCG complex of Angola and Namibia. Precambr. Res. 379, 106821. https://doi.org/10.1016/j.precamres.2022.106821.
Miller, R.McG., 2008. The Geology of Namibia, vol. 1, Archaean to Mesoproterozoic. Ministry of Mines and Energy, Geological Survey, Windhoek, Namibia, 631 p.
Miller, C.F., McDowell, S.M., Mapes, R.W., 2003. Hot and cold granites? Implications of zircon saturation temperatures and preservation of inheritance. Geology 31, 529–532.
Mochales, T., Merino-Martínez, E., Rey-Moral, C., Machadinho, A., Carvalho, J., Represas, P., García-Lobón, J.L., Feria, M.C., Martín-Banda, R., López-Bahut, M.T., Alves, D., Ramalho, E., Manuel, J., Cordeiro, D., 2025. Detailed in-depth mapping of the world largest anorthositic complex: magnetic anomalies, 2.5-3D modelling and emplacement constraints of the Kunene complex (KC), SW Angola. Geosci. Front. 16 (3), 102030. https://doi.org/10.1016/j.gsf.2025.102030.
Morais, E., Sinigoi, S., Mayer, A., Mucana, A., Miguel, L.G., Neto, J., 1998. The Kunene Gabbro-anorthosite complex: preliminary results based on new field and chemical data. Africa Geoscience Review 5, 14.
Nelson, D.A., Cottle, J.M., 2018. The secular development of accretionary orogens: linking the Gondwana magmatic arc record of West Antarctica, Australia and South America. Gondw. Res. 63, 15–33.
Pascal, M., 1980. Etude géologique des formations précambriennes du haut-plateau méridional de l'Angola. Unpublished Ph.D. Thesis, Université Scientifique et Medicale de Grenoble, 351 p.
Pearce, J.A., 2008. Geochemical fingerprinting of oceanic basalts with applications to ophiolite classification and the search for Archean oceanic crust. Lithos 100, 14–48. https://doi.org/10.1016/j.lithos.2007.06.016.
Pearce, T.H., Gorman, B.E., Birkett, T.C., 1977. The relationship between major element geochemistry and tectonic environment of basic and intermediate volcanic rocks. Earth Planet Science Letters 36, 121–132. https://doi.org/10.1016/0012-821X(77)90193-5.
Pearce, J.A., Harris, N.W., Tindle, A.G., 1984. Trace element discrimination diagrams for the tectonic interpretation of granitic rocks. J. Petrol. 25, 956–983. https://doi.org/10.1093/petrology/25.4.956.
Pedreira, A.J., De Waele, B., 2008. Contemporaneous evolution of the Palaeoproterozoic–Mesoproterozoic sedimentary basins of the São Francisco–Congo Craton. Geol. Soc. Lond. Spec. Publ. 294, 33–48. https://doi.org/10.1144/SP294.3.
Pereira, E., Tassinari, C.G., Rodrigues, J.F., Van-Dúnen, V., 2011. New data on the deposition age of the volcano-sedimentary Chela Group and its Eburnean basement: implications to post- Eburnean crustal evolution of the SW of Angola. Comunicações Geológicas Do LNEG 98, 29–40.
Pereira, E., Rodrigues, J.F., Tassinari, C., Van-Dúnen, M.V., 2013. Geologia da região de Lubango, SW de Angola. Evolução no contexto do cratão do Congo. Laboratório Nacional de Energia e Geologia, (LNEG), Portugal. Instituto Geológico de Angola (IGEO). 164 p.
Polat, A., Frei, R., Deng, D., Yang, X.M., Sotiriou, P., 2022. Anatomy of a Neoarchean continental arc-backarc system in the Cross Lake-Pipestone Lake region, northwestern Superior Province. Canada. Precambrian Research 30, 106556. https://doi.org/10.1016/j.precamres.2021.106556.
Potti, J., 2021. Carta Geológica de Angola à escala 1:250.000, Folha Sul D-33/P, Matala, e Notícia Explicativa. Ministério dos Recursos Minerais, Petróleo e Gás, UTE PLANAGEO (IGME-LNEG-Impulso) - Instituto Geológico de Angola (IGEO), Luanda, Angola, 159 p.
Potti, J., Merino-Martínez, E., Goicoechea, P.P., 2021. Carta Geológica de Angola à escala 1:250.000, Folhas Sul E-33/B e Sul E-33/H, Oncócua, e Notícia Explicativa. Ministério dos Recursos Minerais, Petróleo e Gás, UTE PLANAGEO (IGME-LNEG-Impulso) - Instituto Geológico de Angola (IGEO), Luanda, Angola, 173 p.
Profeta, L., Ducea, M.N., Chapman, J.B., Paterson, S.R., Gonzales, S.M.H., Kirsch, M., Petrescu, L., Decelles, P.G., 2015. Quantifying crustal thickness over time in magmatic arcs. Sci. Rep. 5, 17786. https://doi.org/10.1038/srep17786.
Rey-Moral, C., Mochales, T., Merino Martínez, E., García Lobón, J.L., López Bahut, M.T., Martín-Banda, R., Feria, M.C., Ballesteros, D., Machadinho, A., Alves, D., 2022. Recording the largest gabbro-anorthositic complex worldwide: the Kunene complex (KC). SW Angola. Precambrian Research 379, 106790. https://doi.org/10.1016/j.precamres.2022.106790.
Roberts, N.M.W., 2013. The boring billion? Lid tectonics, continental growth and environmental change associate with the Columbia supercontinent. Geosci. Front. 4, 681–691.
Roberts, N.M.W., Condie, K.C., Palin, R.M., Spencer, C.J., 2023. Hot, Wide, Continental Back-arcs Explain Earth's Enigmatic mid-Proterozoic Magmatic and Metamorphic Record. Tektonika 1 (1), 67–75. https://doi.org/10.55575/tektonika2023.1.1.32.
Rodrigues, J. F., Merino Martínez, E., Ferreira, E. (coords.), 2021. Mapa Tectónico de Angola à escala 1:1.100.000, e Notícia Explicativa. Ministério dos Recursos Minerais, Petróleo e Gás, UTE PLANAGEO (IGME-LNEG-Impulso) - Instituto Geológico de Angola (IGEO), Luanda, Angola, 101 p.
Saccani, E., 2015. A new method of discriminating different types of post-Archean ophiolitic basalts and their tectonic significance using Th-Nb and Ce-Dy-Yb systematics. Geosci. Front. 6, 481–501. https://doi.org/10.1016/j.gsf.2014.03.006.
Salminen, J., Hanson, R., Evans, D.A.D., Gong, Z., Larson, T., Walker, O., Gumsley, A., Söderlund, U., Ernst, R., 2018. Direct Mesoproterozoic connection of the Congo and

Kalahari cratons in proto-Africa: strange attractors across supercontinental cycles. Geology 46, 1011–1014. https://doi.org/10.1130/G45294.1.
Seth, B., Kröner, A., Mezger, K., Nemchin, A.A., Pidgeon, R.T., Okrusch, M., 1998. Archaean to Neoproterozoic magmatic events in the Kaoko belt of NW Namibia and their geodynamic significance. Precambr. Res. 92, 341–363. https://doi.org/10.1016/S0301-9268(98)00086-2.
Seth, B., Armstrong, R.A., Brandt, S., Villa, I.M., Kramers, J.D., 2003. Mesoproterozoic U–Pb and Pb–Pb ages of granulites in NW Namibia: reconstructing a complete orogenic cycle. Precambr. Res. 126, 147–168. https://doi.org/10.1016/S0301-9268(03)00193-1.
Seth, B., Armstrong, R.A., Büttner, A., Villa, I.M., 2005. Time constraints for Mesoproterozoic upper amphibolite facies metamorphism in NW Namibia: a multi-isotopic approach. Earth Planet. Sci. Lett. 230, 355–378. https://doi.org/10.1016/j.epsl.2004.11.022.
Siga Jr, O., Stipp Basei, M.A., Nutman, A., Sato, K., McReath, I., Passarelli, C.R., Lliu, D., 2011. Extensional and Colisional Magmatic Records in the Apiaí Terrane, South-Southeastern Brazil: Integration of Geochronological U-Pb Zircon Ages. Revista do Instituto de Geociências – USP, Geol. USP, Sér. cient., São Paulo, v. 11, n. 3, p. 149-175. www.igc.usp.br/geologiausp.
Silva, Z.C.G., 1990. Geochemistry of the Gabbro-Anorthosite complex of Southwest Angola. J. Afr. Earth Sc. 10 (4), 683–692.
Silva, A.F., 2005. A Geologia da República de Angola desde o Paleoarcaico ao Paleozóico Inferior. Instituto Nacional de Engenharia, Tecnologia e Inovação, IP, p. 44.
Silva, P.B., Caessa, P., 2021. Carta Geológica de Angola à escala 1:250.000, Folha Sul D-33/I, Cubal, e Notícia Explicativa. Ministério dos Recursos Minerais, Petróleo e Gás, UTE PLANAGEO (IGME-LNEG-Impulso) - Instituto Geológico de Angola (IGEO), Luanda, Angola, 179 pp.
Silva, A.T.F., Simões, M.V.C., 1980. Geologia da região de Caluquembe (Angola). Boletim da Sociedade Geológica de Portugal, Vol. XXII, 363-375.
Silva, A.T.F., Torquato, J.R., Kawashita, K., 1973. Alguns dados geocronológicos pelo método K/Ar da região de Vila Paiva Couceiro, Quilengues e Chicomba (Angola). Serviço De Geologia e Minas De Angola 24, 29–46.
Silva, P.B., Oliveira, A., Duarte, L., Labaredas, J., Goicoechea, P., 2021. Carta Geológica de Angola à escala 1:250.000, Folha Sul D-33/T, Chibia, e Notícia Explicativa. Ministério dos Recursos Minerais, Petróleo e Gás, UTE PLANAGEO (IGME-LNEG-Impulso) - Instituto Geológico de Angola (IGEO), Luanda, Angola, 255 p.
Simon, S.J., Wei, C., Ellmies, R., Yang, H., Soh Tamehe, L., 2017. New SIMS U-Pb age on zircon from the Epembe carbonatite dyke, NW Namibia: Implications for Mesoproterozoic evolution of carbonatites at the southern margin of the Congo Craton. J. Afr. Earth Sc. 135, 108–114. https://doi.org/10.1016/j.jafrearsci.2017.08.011.
Sizova, E., Gerya, T., Brown, M., Perchuk, L.L., 2010. Subduction styles in the precambrian: Insight from numerical experiments. Lithos 116 (3), 209–229. https://doi.org/10.1016/j.lithos.2009.05.028.
Slagstad, T., Henderson, I.H.C., Roberts, N.M.W., Kulakov, E.V., Ganerød, M., Kirkland, C.L., Dalslåen, B., Creaser, R.A., Coint, N., 2022. Anorthosite formation and emplacement coupled with differential tectonic exhumation of ultrahigh-temperature rocks in a Sveconorwegian continental back-arc setting. Precambr. Res. 376, 106695. https://doi.org/10.1016/j.precamres.2022.106695.
Slejko, F.F., Demarchi, G., Morais, E., 2002. Mineral chemistry and Nd isotopic composition of two anorthositic rocks from the Kunene complex, South Western Angola. J. Afr. Earth Sc. 35, 77–88. https://doi.org/10.1016/S0899-5362(02)00007-6.
Smithies, H., Howard, H.M., Evins, P.M., Kirkland, C.L., Kelsey, D.E., Hand, M., Wingate, M.T.D., Collins, A.S., Belousova, E.A., 2011. High-temperature granite magmatism, crust-mantle interaction and the Mesoproterozoic intracontinental evolution of the Musgrave Province, Central Australia. J. Petrol. 52 (5), 931–958. https://doi.org/10.1093/petrology/egr010.
Smits, R.G., Collins, W.J., Hand, M., Dutch, R., Payne, J., 2014. A Proterozoic Wilson cycle identified by Hf isotopes in central Australia: Implications for the assembly of Proterozoic Australia and Rodinia. Geology 42 (3), 231–234. https://doi.org/10.1130/G35112.1.
Sotiriou, P., Polat, A., 2023. Petrogenesis of anorthosites throughout Earth history. Precambr. Res. 384, 106936. https://doi.org/10.1016/j.precamres.2022.106936.
Sousa, J.C., Oliveira, A., Máximo, J., 2021. Carta Geológica de Angola à escala 1: 250.000, Folha Sul D-33/Q, Jamba, e Notícia Explicativa. Ministério dos Recursos Minerais, Petróleo e Gás, UTE PLANAGEO (IGME-LNEG-Impulso) - Instituto Geológico de Angola (IGEO), Luanda, Angola, 257 p.
Sun, S.S., McDonough, W.F., 1989. Chemical and isotopic systematics of oceanic basalts: implications for mantle composition and processes. In: Saunders, A.D., Norry, M. (eds), Magmatism in Ocean Basins. Geological Society of London Special Publications 42, pp 313–345. DOI: 10.1144/GSL.SP.1989.042.01.19.
Tack, L., Wingate, M.T.D., De Waele, B., Meert, J., Belousova, E., Griffin, B., Tahon, A., Fernandez-Alonso, M., 2010. The 1375 Ma "Kibaran event" in Central Africa: Prominent emplacement of bimodal magmatism under extensional regime. Precambr. Res. 180, 63–84. https://doi.org/10.1016/j.precamres.2010.02.022.
Torquato, J.R., 1974. Considerações sobre a idade absoluta do Grupo Chela. Dir. Prov. Serviço Geologia e Minas, Angola, Memória 14, 10 p.
Torquato, J.R., 1977. Geotectonic outline of Angola. Cahiers O.R.S.T.O.M., Sér. Géol., vol. IX, n° 1/2, 15–34.
Torquato, J.R., Allsopp, H.L., 1973. Rubidium-strontium geochronology of granitic rocks from the Morro Vermelho area (Tiger Bay, Angola). Geol. Rundsch. 62, 172–179. https://doi.org/10.1007/BF01826824.
Torquato, J.R., Amaral, G., 1973. Idades K/Ar em rochas das regiões de Catanda e Vila do Almoster. Bol. Inst. Invest. Cient., Angola (Luanda), vol. 10, Pub. IICA, 308.
Torquato, J.R., Salgueiro, M.A.A., 1977. Sobre a idade de algumas rochas da região da Cahama (Folha Geológica n° 399): Angola. Boletim IG. Instituto De Geociências, USP 8, 97–106. https://doi.org/10.11606/ISSN.2316-8978.V8I0P97-106.
Torquato, J.R., da Silva, A.T.S.F., Cordani, U.G., Kawashita, K., 1979. Evolução geológica do cinturão móvel do Quipungo no Ocidente de Angola. Anais Da Academia Brasileira De Geociências. 51 (1), 133–144.
Tshiningayamwe, M., Bolhar, R., Nex, P.A.M., 2022a. Petrology, geochemistry and new U–Pb ages of the Epembe syenites and carbonatite, northwest Namibia. J. Afr. Earth Sc. 196, 104719. https://doi.org/10.1016/j.jafrearsci.2022.104719.
Tshiningayamwe, M., Bolhar, R., Nex, P.A.M., Ueckermann, H., Chang, Q., 2022b. An apatite trace element and Sr-Nd isotope geochemical study of syenites and carbonatite, exemplified by the Epembe alkaline-carbonatite complex, Namibia. Lithos 420–421, 106699. https://doi.org/10.1016/j.lithos.2022.106699.
Vermaak, C.F., 1981. Kunene Anorthosite complex. In: Hunter, D.R. (Ed.), Precambrian of the Southern Hemisphere (developments in Precambrian Geology), 2. Elsevier, Amsterdam, pp. 578–599.
Verma, S.P., Guevara, M., Agrawal, S., 2006. Discriminating four tectonic settings: five new geochemical diagrams for basic and ultrabasic volcanic rocks based on log-ratio transformation of major-element data. J. Earth Syst. Sci. 115, 485–528. https://doi.org/10.1007/BF02702907.
Vermeesch, P., 2012. On the visualisation of detrital age distributions. Chem. Geol. 312–313, 190–194. https://doi.org/10.1016/j.chemgeo.2012.04.021.
Vermeesch, P., Pease, V., 2021. A genetic classification of the tholeiitic and calc-alkaline magma series. Geochem. Perspect. Lett. 19, 1–6. https://doi.org/10.7185/geochemlet.2125.
Wang, Z., Wang, Z., Zhang, Y., Xu, B., Li, Y., Tiang, Y., Wang, Y., Peng, J., 2022. Linking ~1.4–0.8 Ga volcano-sedimentary records in eastern Central Asian orogenic belt with southern Laurentia in supercontinent cycles. Gondw. Res. 105, 416–431. https://doi.org/10.1016/j.gr.2021.09.019.
Whalen, J.B., Currie, K.L., Chappell, B.W., 1987. A-type granites: geochemical characteristics, discrimination and petrogenesis. Contrib. Miner. Petrol. 95, 407–419. https://doi.org/10.1007/BF00402202.